Supporting Information

Metal – organic – framework - derived Co_9S_8@CoS@CoO@C nanoparticles as efficient electro- and photo-catalysts for oxygen evolution reaction

Jiying Long, [a]Yun Gong*[a] and Jianhua Lin*[ab]

[a]*Department of Applied Chemistry, College of Chemistry and Chemical Engineering, Chongqing University, Chongqing 401331, P. R. China Tel: +86-023-65678932 *E-mail: gongyun7211@cqu.edu.cn*

[b]*State Key Laboratory of Rare Earth Materials Chemistry and Applications, College of Chemistry and Molecular Engineering, Peking University, Beijing 100871, P. R. China Tel: +86-010-62753541 *E-mail: jhlin@pku.edu.cn*

Calculation Method. Details concerning the calculation of mass activity and specific activity are shown below.[1]

The values of mass activity ($A\cdot g^{-1}$) were calculated from the catalyst loading m ($0.2\ mg\cdot cm_{geo}^{-2}$) and the measured current density j ($mA\cdot cm_{geo}^{-2}$) at E = 1.38 V vs. RHE:

$$\text{mass activity} = j/m \qquad (1)$$

The values of specific activity ($mA\cdot cm^{-2}$) were calculated from the BET surface area S_{BET} ($m^2\cdot g^{-1}$), catalyst loading m ($0.2\ mg\cdot cm_{geo}^{-2}$), and the measured current density j ($mA\cdot cm_{geo}^{-2}$) at E = 1.38 V vs. RHE:

$$\text{specific activity} = j/(10\cdot S_{BET}\cdot m) \qquad (2)$$

(a)

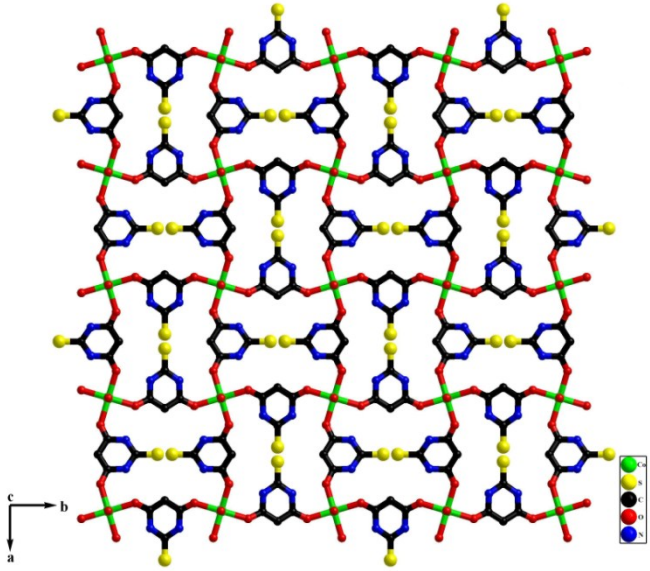

(**b**)

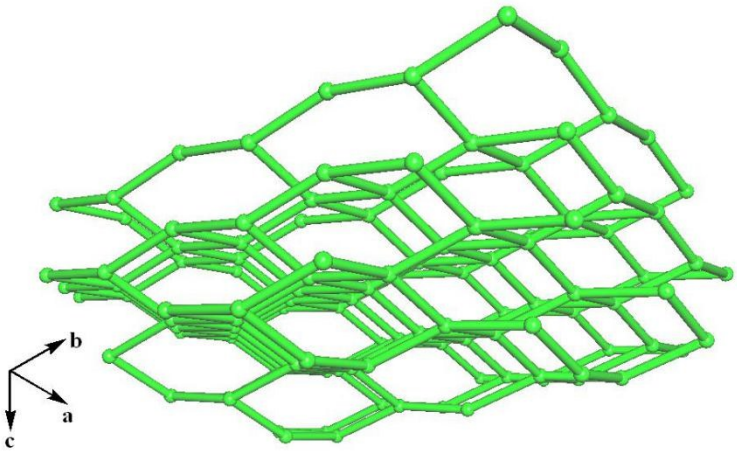

Fig. S1 3D architecture of the Co-MOF (H atoms omitted for clarity) (**a**); Schematic illustrating the diamondoid topology of the Co-MOF (**b**).

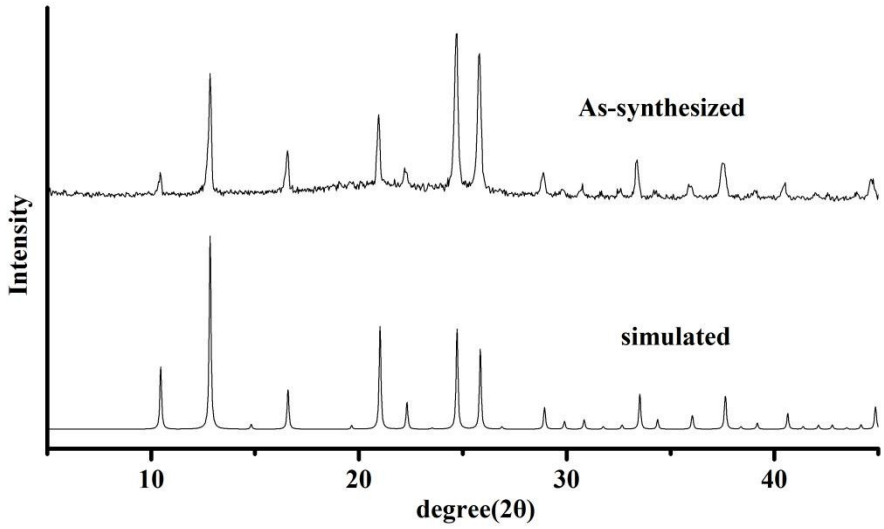

Fig. S2 The PXRD pattern of the Co-MOF.

(a) **(b)**

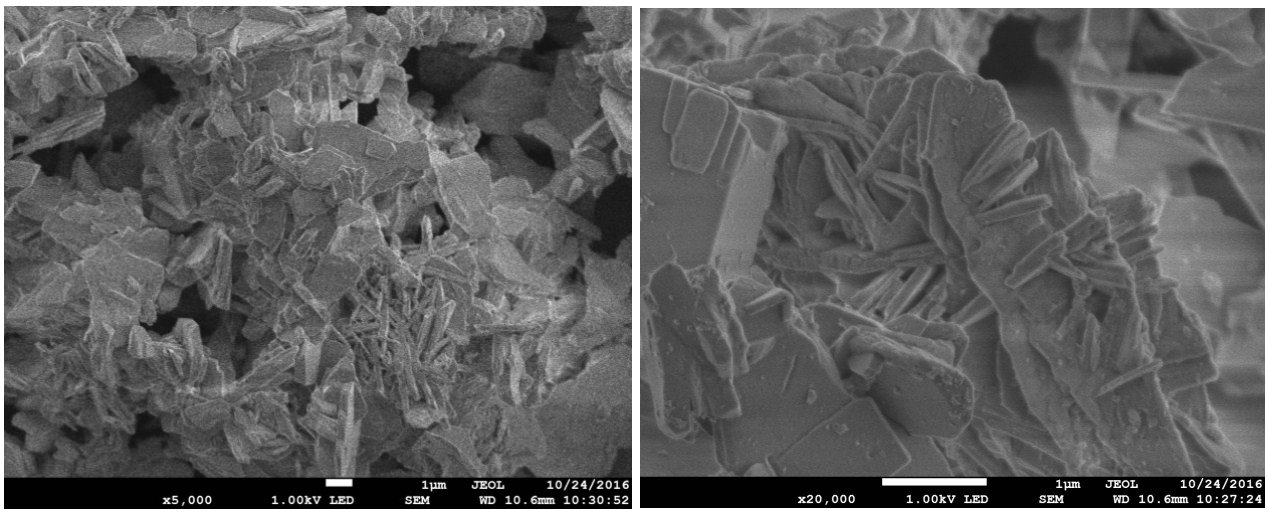

Fig. S3 The SEM images of the Co-MOF at different magnifications (**a**, **b**).

(a) **(b)**

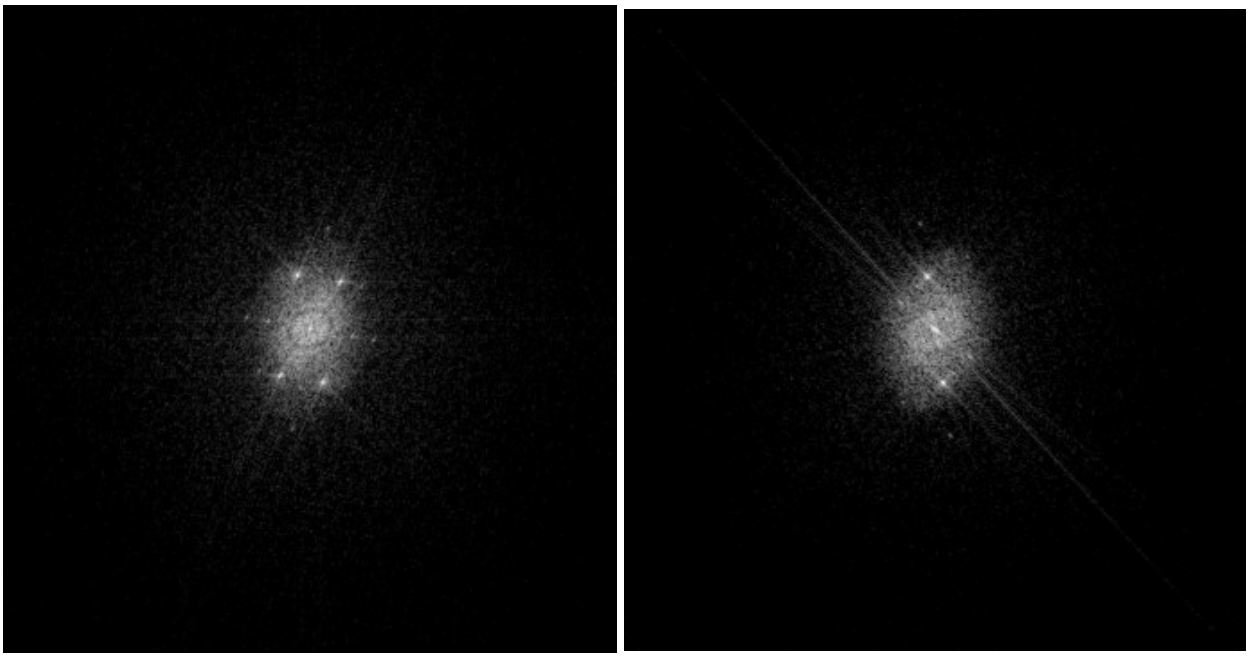

(c)

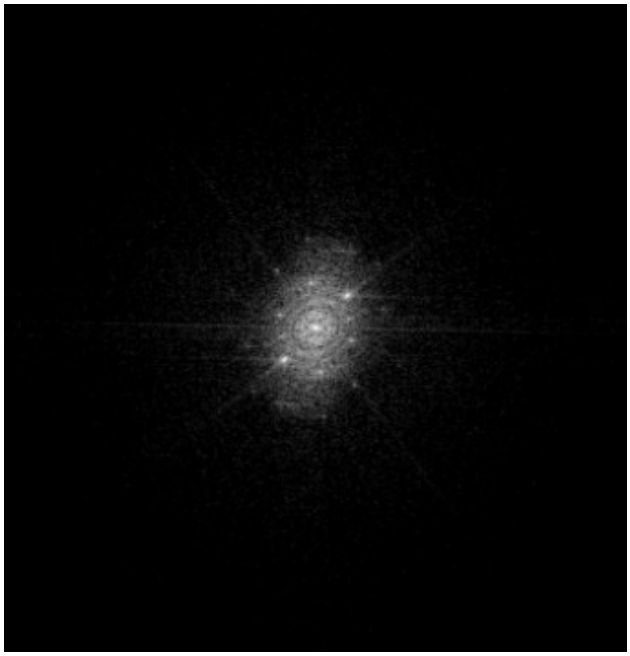

Fig. S4 The corresponding FFT images (**a-c**) of the HRTEM in **Fig. 4a-d** for the as-synthesized Co_9S_8@CoS@CoO@C NPs.

(a) **(b)**

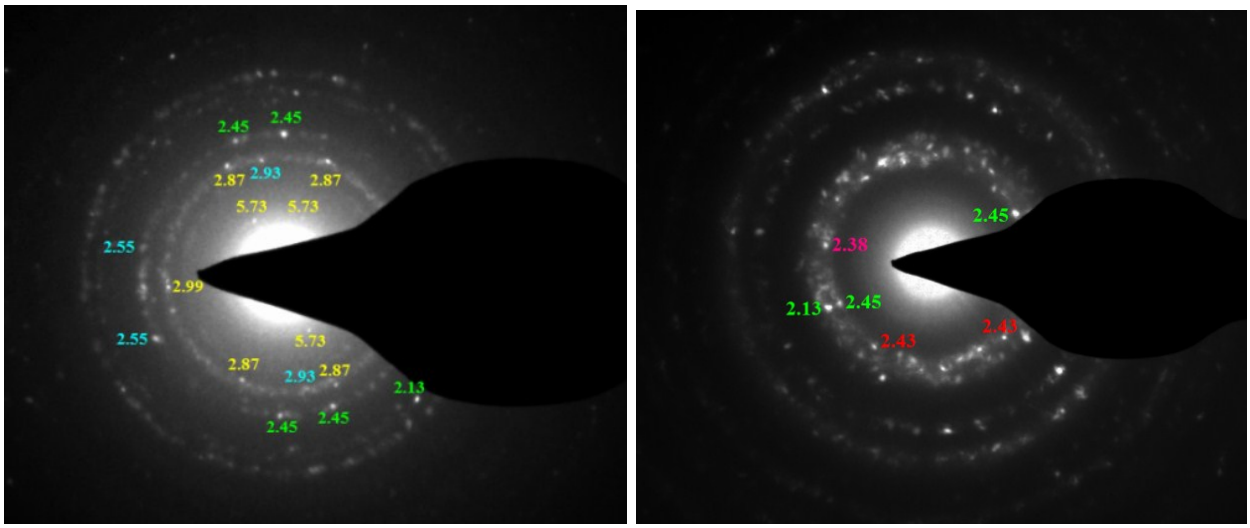

Fig. S5 The SAED of the as-synthesized Co_9S_8@CoS@CoO@C NPs before (**a**) and after 6h-electrolysis experiment at E = 1.38 V vs RHE (**b**).

(a)

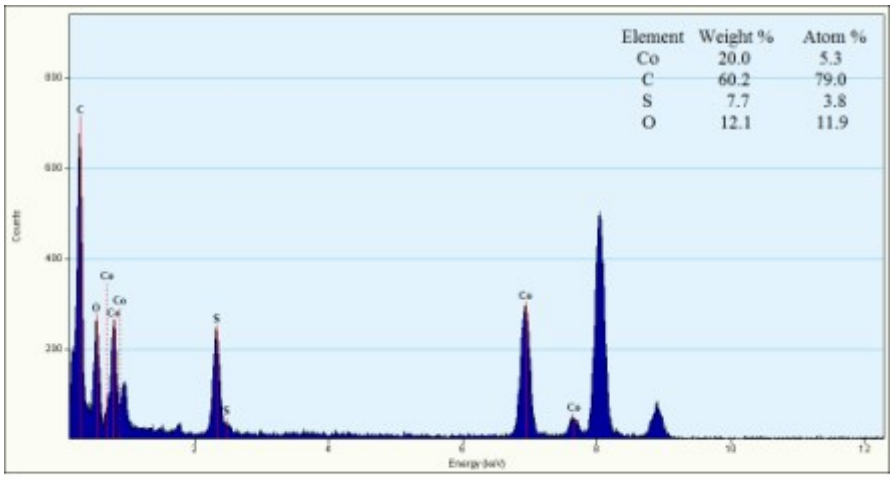

(b)

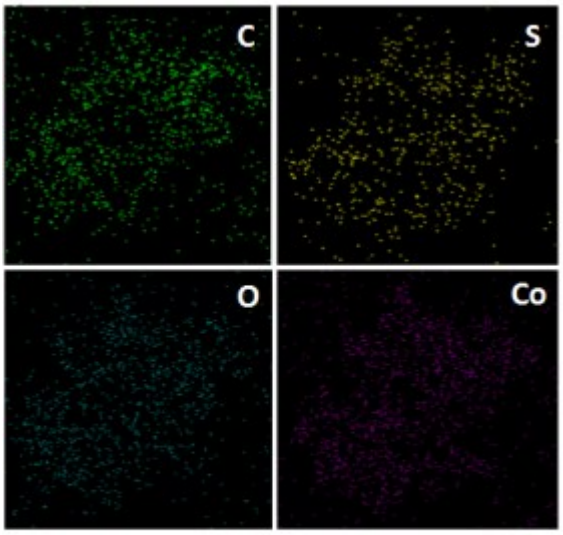

(c)

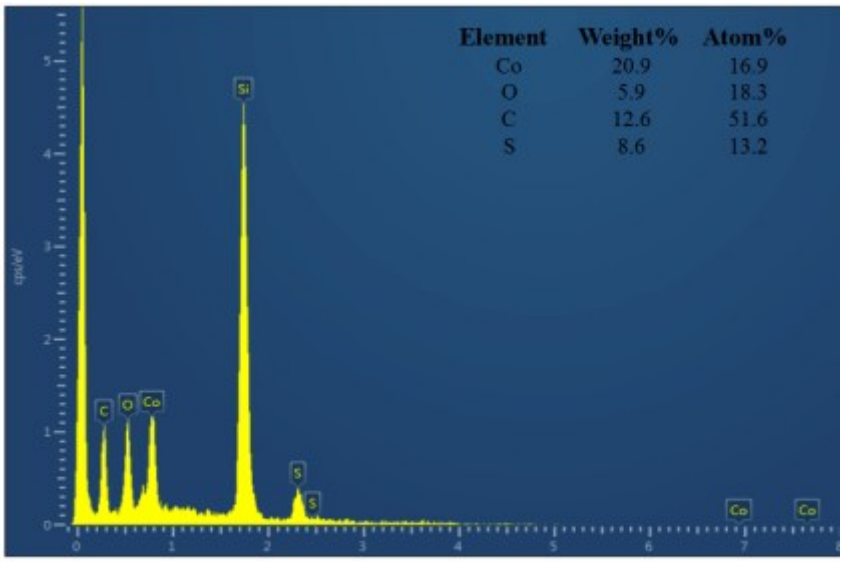

Fig. S6 EDS **(a, c)** and the C, S, O, and Co elemental mappings for the Co_9S_8@CoS@CoO@C NPs **(b)**.

(a)

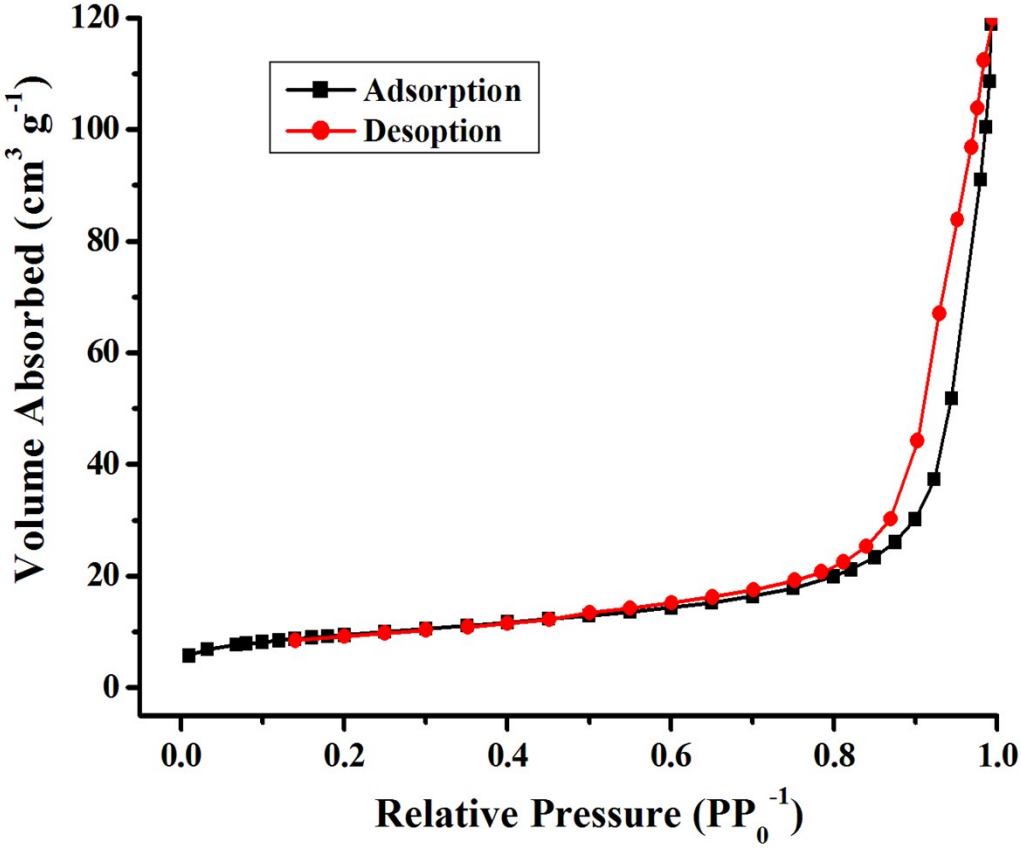
Adsorption
Desoption
Volume Absorbed (cm3 g-1)
Relative Pressure (PP0-1)
0
20
40
60
80
100
120
0.0
0.2
0.4
0.6
0.8
1.0

(b)

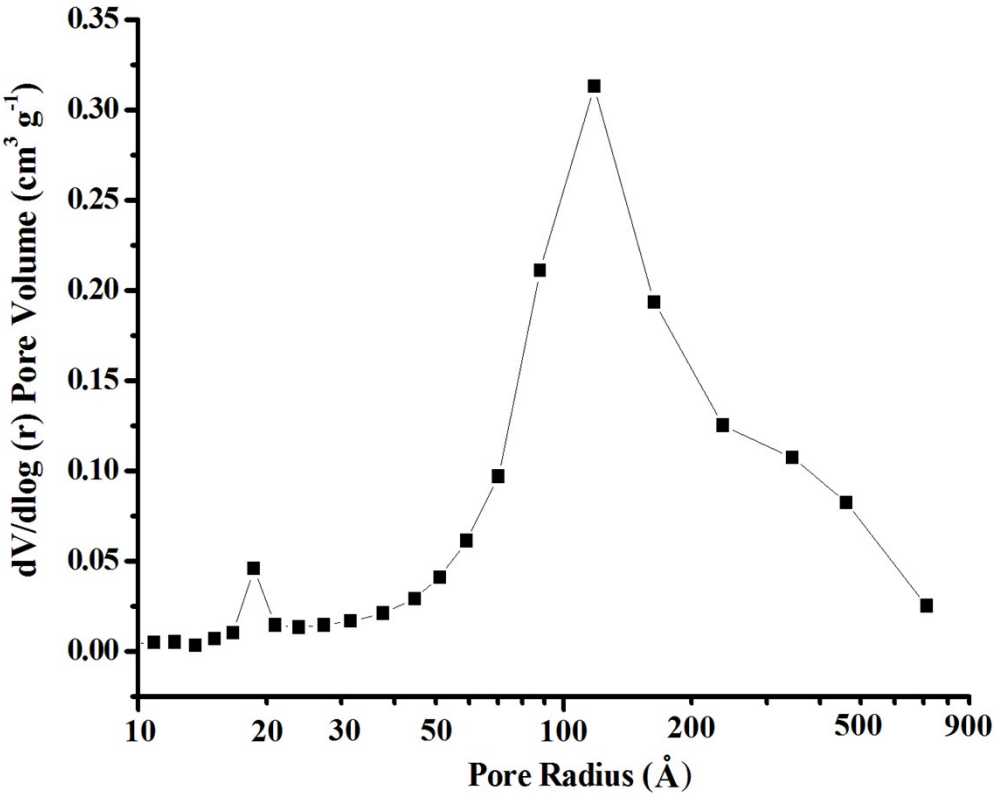
dV/dlog (r) Pore Volume (cm3 g-1)
Pore Radius (Å)
0.00
0.05
0.10
0.15
0.20
0.25
0.30
0.35
10
20
30
50
100
200
500
900

Fig. S7 Nitrogen adsorption-desorption isotherms **(a)** and the corresponding pore-size distribution curve **(b)** of the Co_9S_8@CoS@CoO@C NPs.

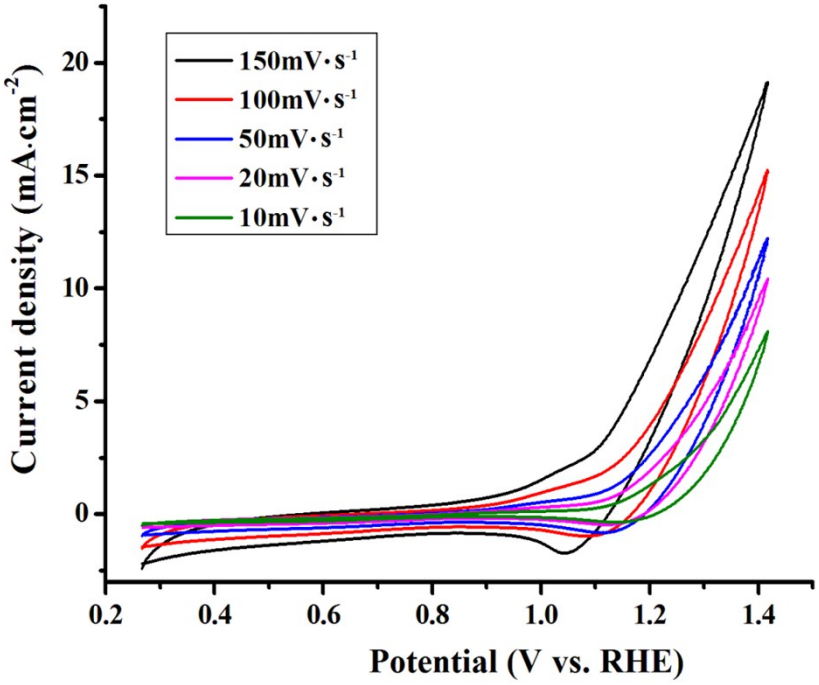

Fig. S8 CVs of the Co_9S_8@CoS@CoO@C NPs recorded after 100 CV cycles in 1 M KOH aqueous solution at a rotating speed of 1600 rpm at various sweep rates from 10 to 150 $mV \cdot s^{-1}$**.**

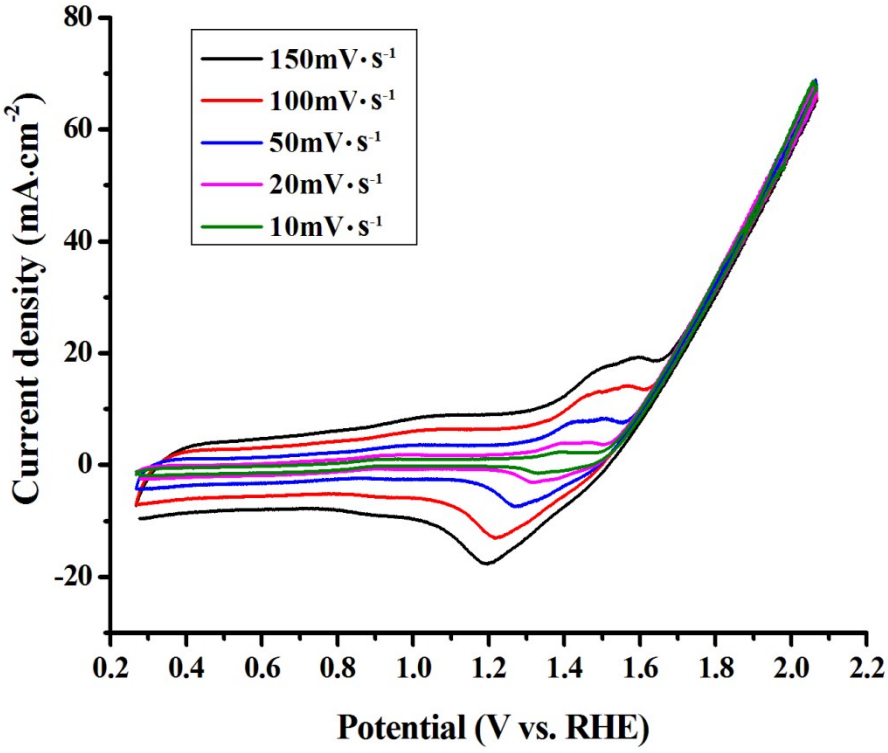

Fig. S9 CVs of RuO_2 in 1 M KOH aqueous solution at a rotating speed of 1600 rpm at various sweep rates from 10 to 150 $mV \cdot s^{-1}$.

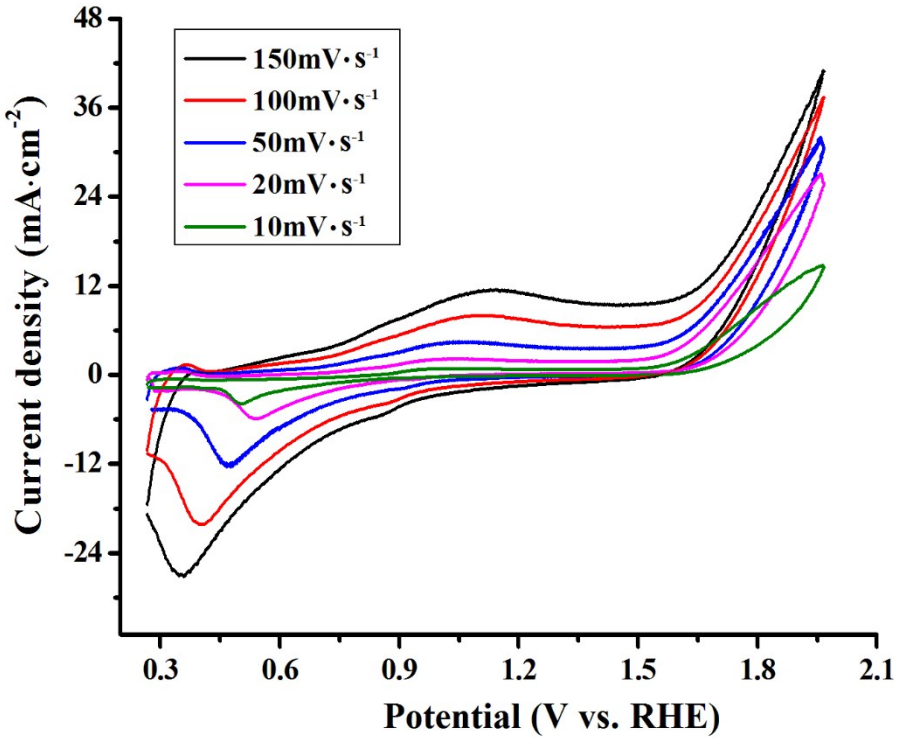

Fig. S10 CVs of Pt in 1 M KOH aqueous solution at a rotating speed of 1600 rpm at various sweep rates from 10

to 150 mV·s^{-1}.

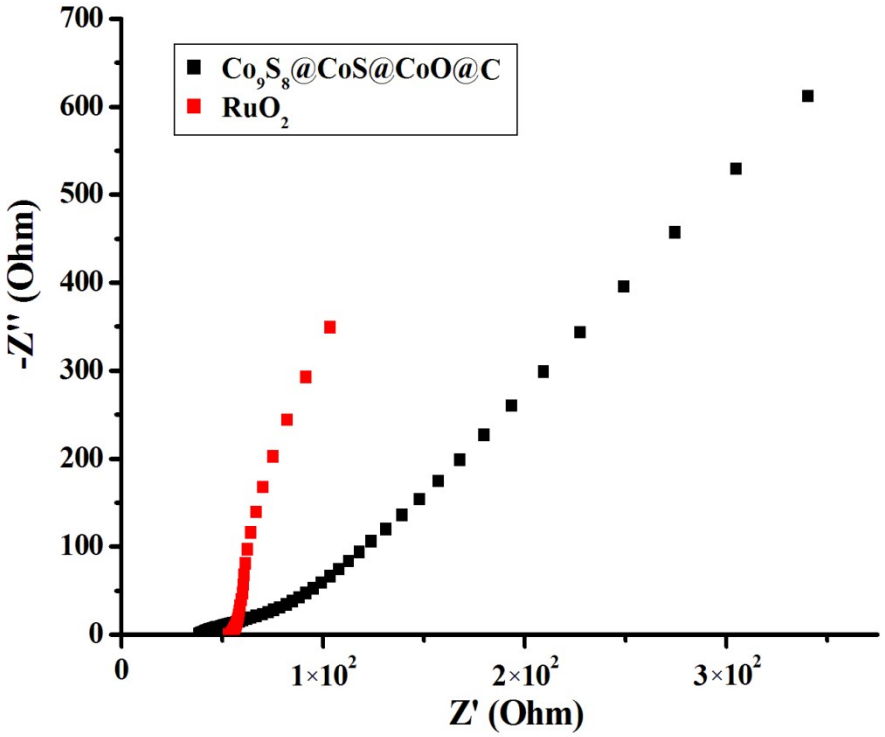

Fig. S11 Nyquist plots of Co_9S_8@CoS@CoO@C recorded after 100 CV cycles and RuO_2 in O_2 saturated 1 M KOH solution at 1.38 V vs. RHE (overpotential η= 0.15 V). Z′ is real impedance and Z″ is imaginary impedance.

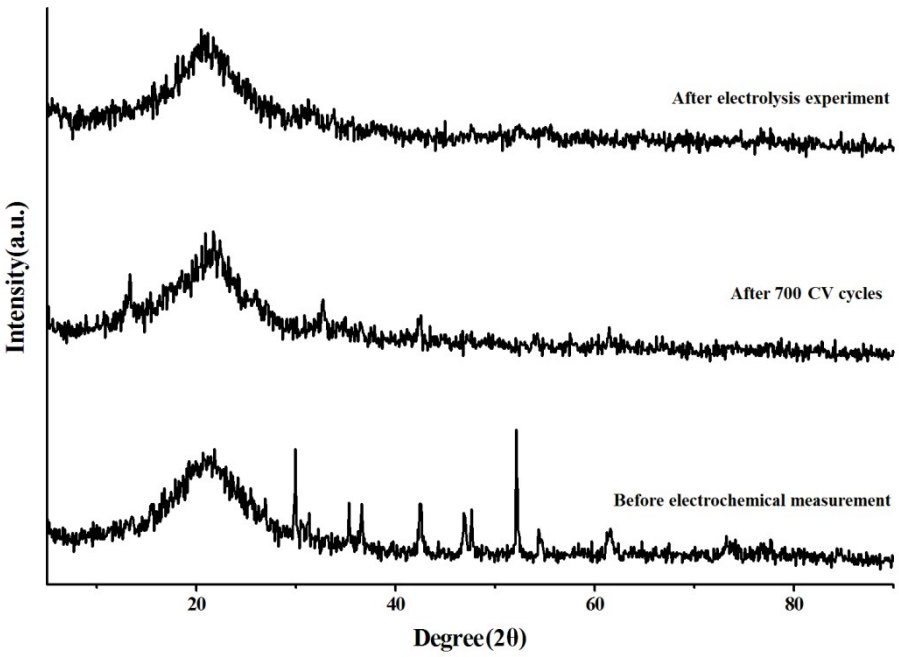

Fig. S12 The PXRD patterns of the Co_9S_8@CoS@CoO@C NPs before (**a**) and after 700 CV cycles in the potential range of 0.25~1.40 V vs. RHE at a scan rate of 150 mV·s^{-1} (**b**); The PXRD pattern of the Co_9S_8@CoS@CoO@C

sample after 6h - electrolysis experiment at *E*= 1.38 V vs. RHE (**c**).

(a)

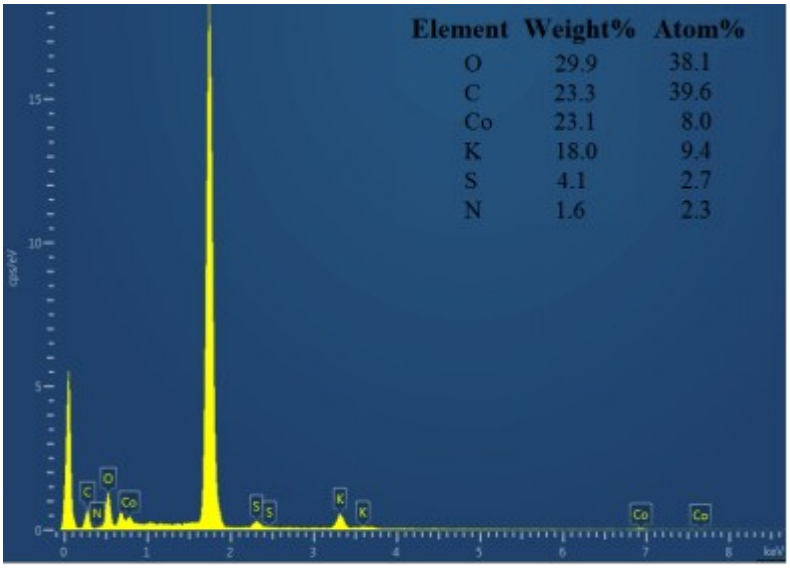

(b)

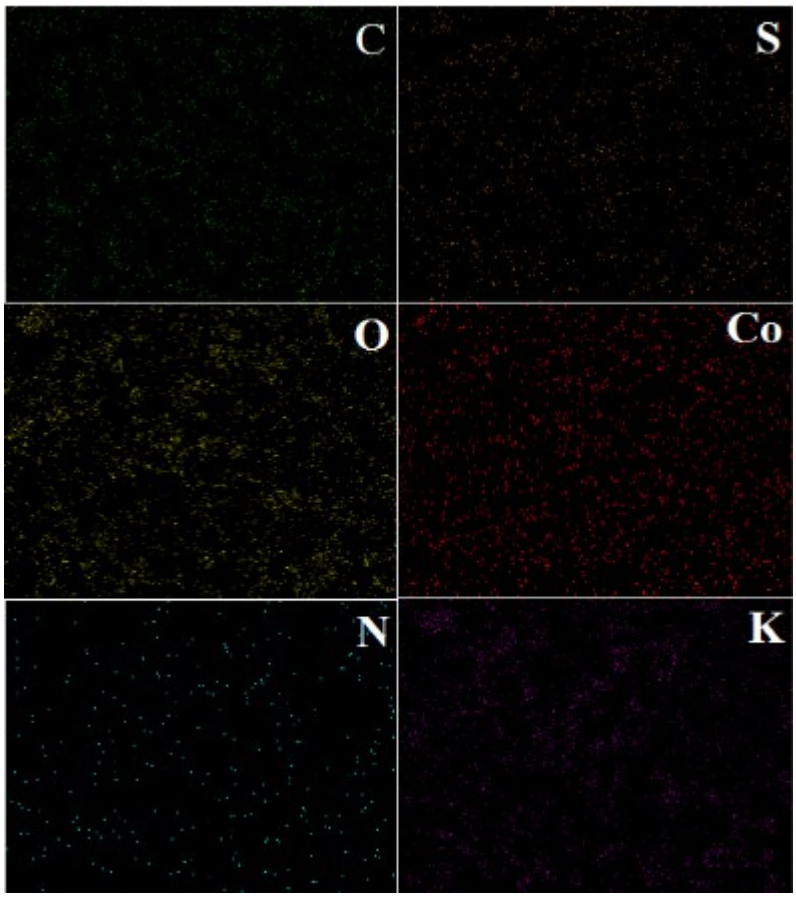

Fig. S13 EDS (**a**) and the C, S, O, Co, N and K elemental mappings for the Co_9S_8@CoS@CoO@C NPs after 700 CV cycles in the potential range of 0.25~1.40 V vs. RHE at a scan rate of 150 mV·s^{-1} (**b**), taking no account of the large amount of Si from the Si substrate.

Table S1 The atom % in the Co_9S_8@CoS@CoO@C catalyst before and after the electrochemical measurement

Atom %	Before electro-chemical measurement	After 700 CV cycles	After 6h-electrolysis experiment	After 12h-electrolysis experiment
Co	5.3 [a] /16.9 [b]	8.0	13.7 [a] /11.5 [b]	10.0 [a] /4.9 [b]
O	11.9 [a] /18.3 [b]	38.1	44.8 [a] /37.8 [b]	53.0 [a] /41.6 [b]
C	79.0 [a] /51.6 [b]	39.6	36.8 [a] /46.0 [b]	28.8 [a] /47.7 [b]
S	3.8 [a] /13.2 [b]	2.7	0.1 [a] /0.2 [b]	/
N	/	2.3	/	/
K	/	9.4	4.6 [a] /4.5 [b]	8.2 [a] /5.8 [b]

[a)] The percentages of the atoms are calculated based on the EDS data in **Fig. S5a**, **Fig. S13a** and **Fig. 14a**.

[b)] The percentages of the atoms are calculated based on the EDS data in **Fig. S5c**, **Fig. S13c** and **Fig. 14c**.

Table S2 The OER current densities (mA·cm^{-2}) at the catalyst-modified Ni foam at different times (Catalyst loading: 5 mg·cm^{-2})

Current density	Co_9S_8@CoS@CoO@C	RuO_2	Pt
Start-up (t = 0)	271.7	183.1	65.8
t=0.06 h	10.36	1.351	0.317
t=0.41 h	4.129	1.084	0.079
t= 3.41 h	5.460	0.868	0.040
t=6 h	4.837	0.756	0.033

(a)

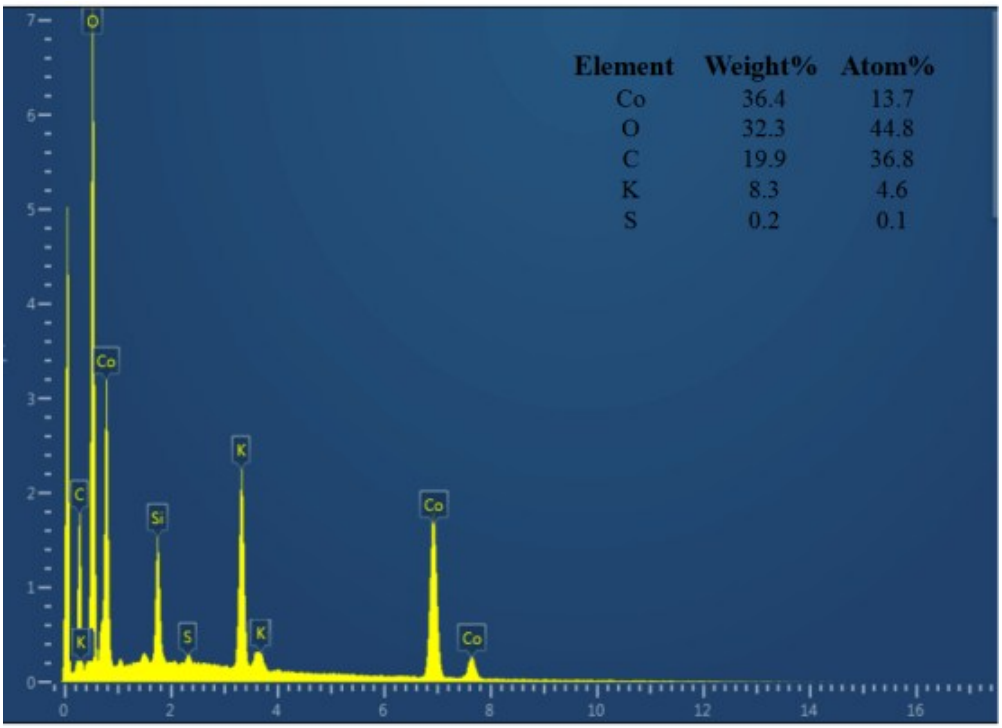
Element Weight% Atom%
Co 36.4 13.7
O 32.3 44.8
C 19.9 36.8
K 8.3 4.6
S 0.2 0.1
O
Co
C
K
Si
S
K
K
Co
Co

(b)

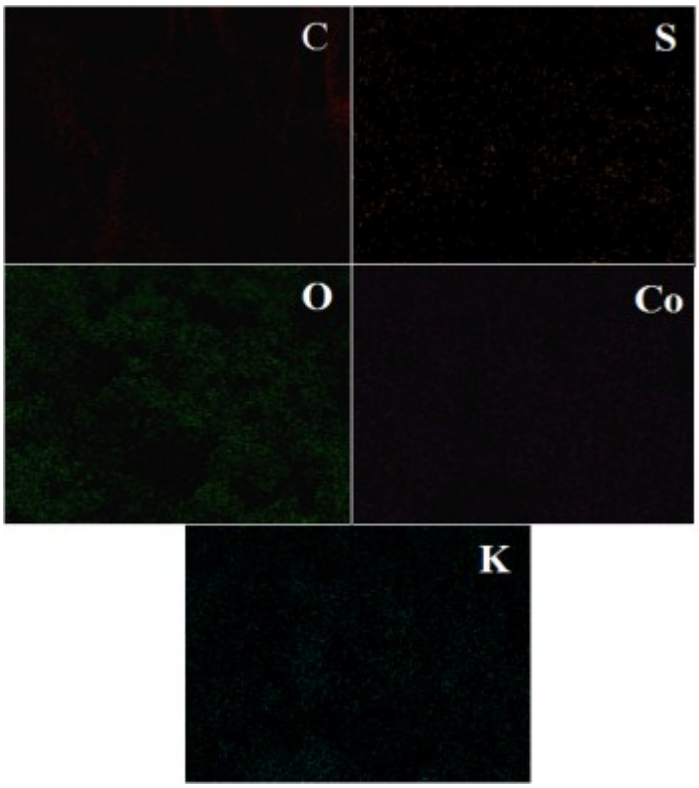
C
S
O
Co
K

(c)

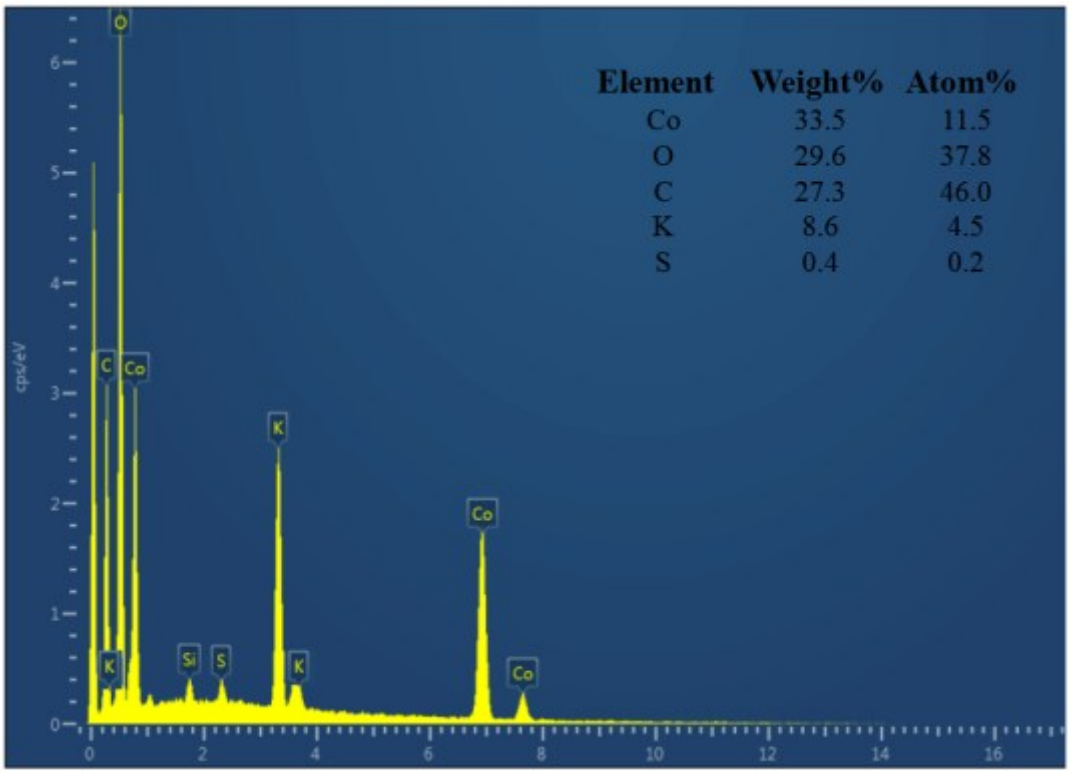

(d)

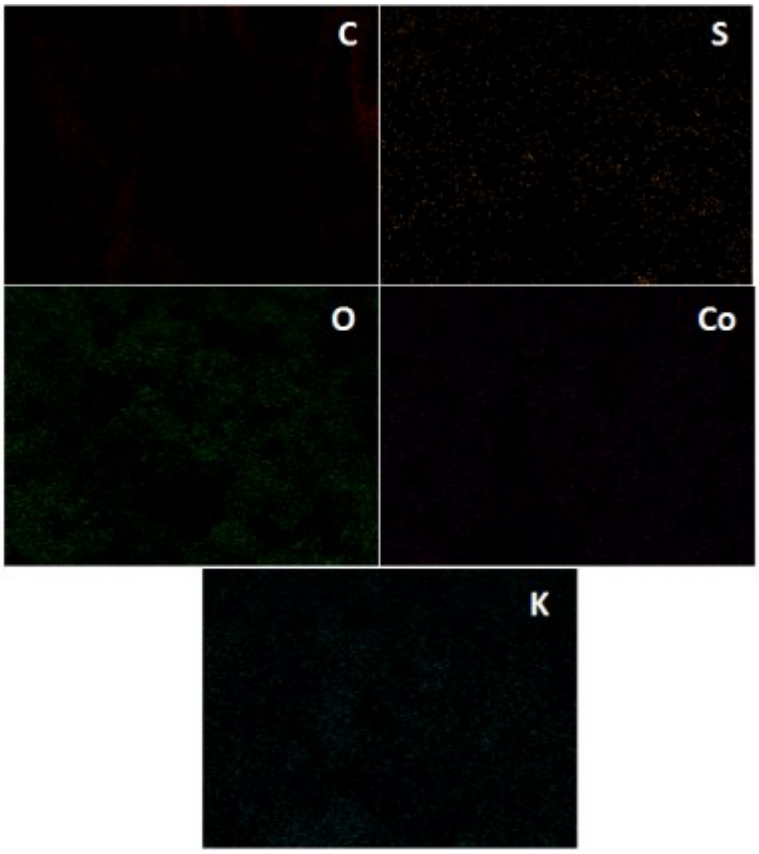

Fig. S14 EDS **(a, c)** and the Co, C, S, O and K elemental mappings for the Co_9S_8@CoS@CoO@C NPs after the 6h-electrolysis experiment **(b, d).**

(a)

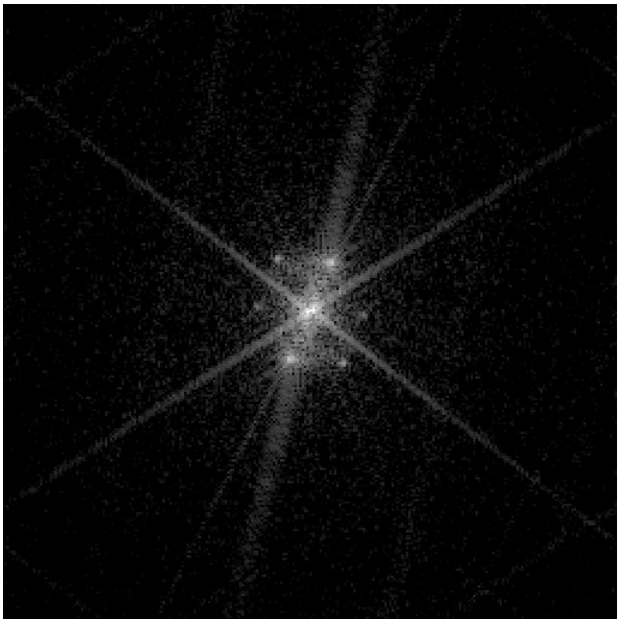

(b)

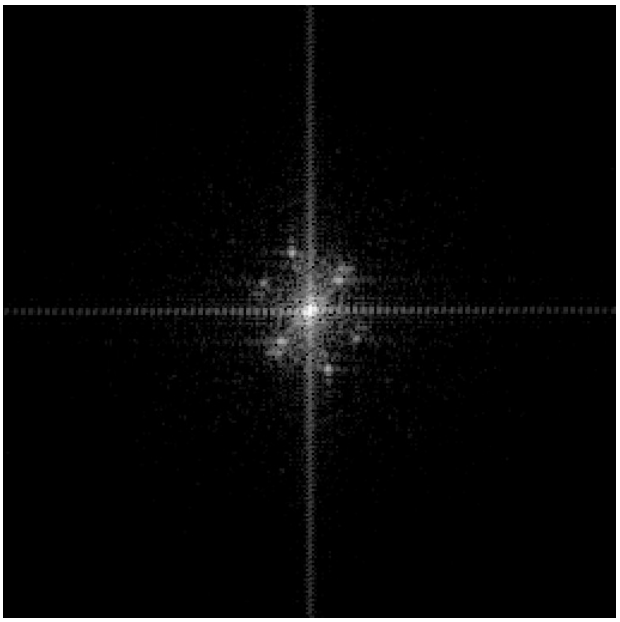

(c)

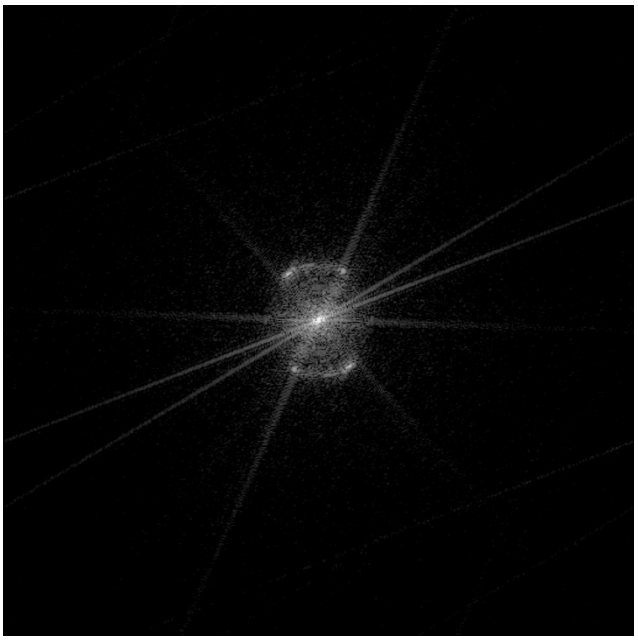

(d)

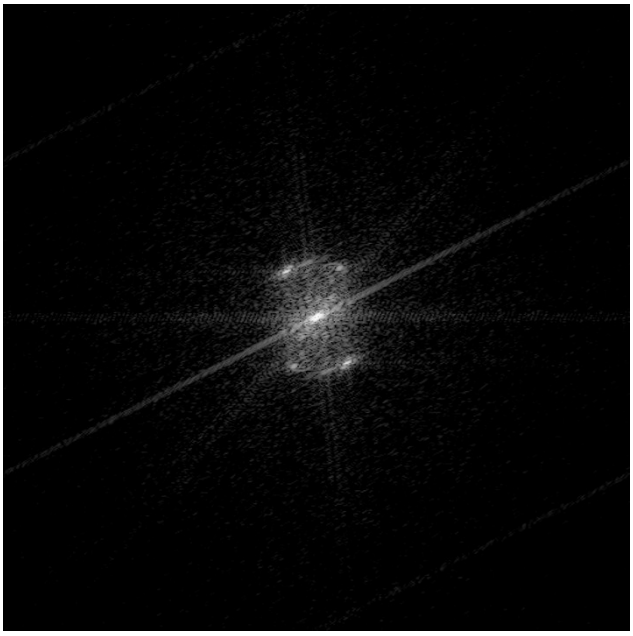

(e)

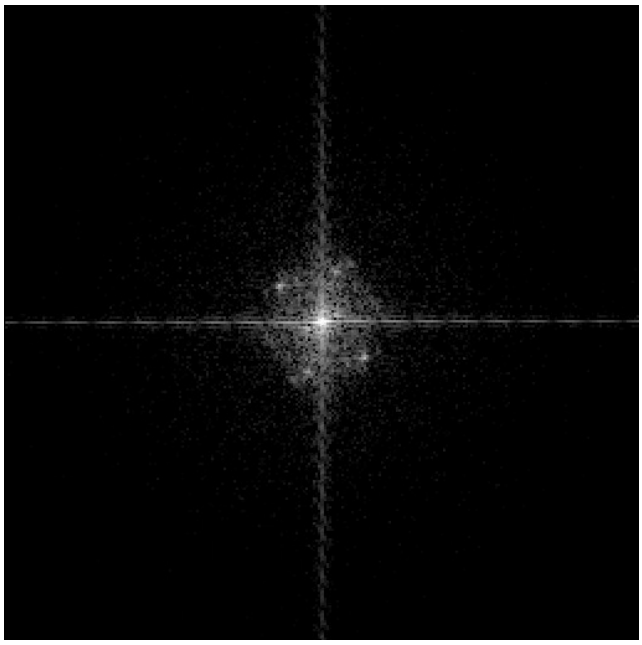

Fig. S15 The corresponding FFT images (**a-e**) of the HRTEM in **Fig. 12a-e** for the Co_9S_8@CoS@CoO@C NPs after the 6h-electrolysis experiment

(a)

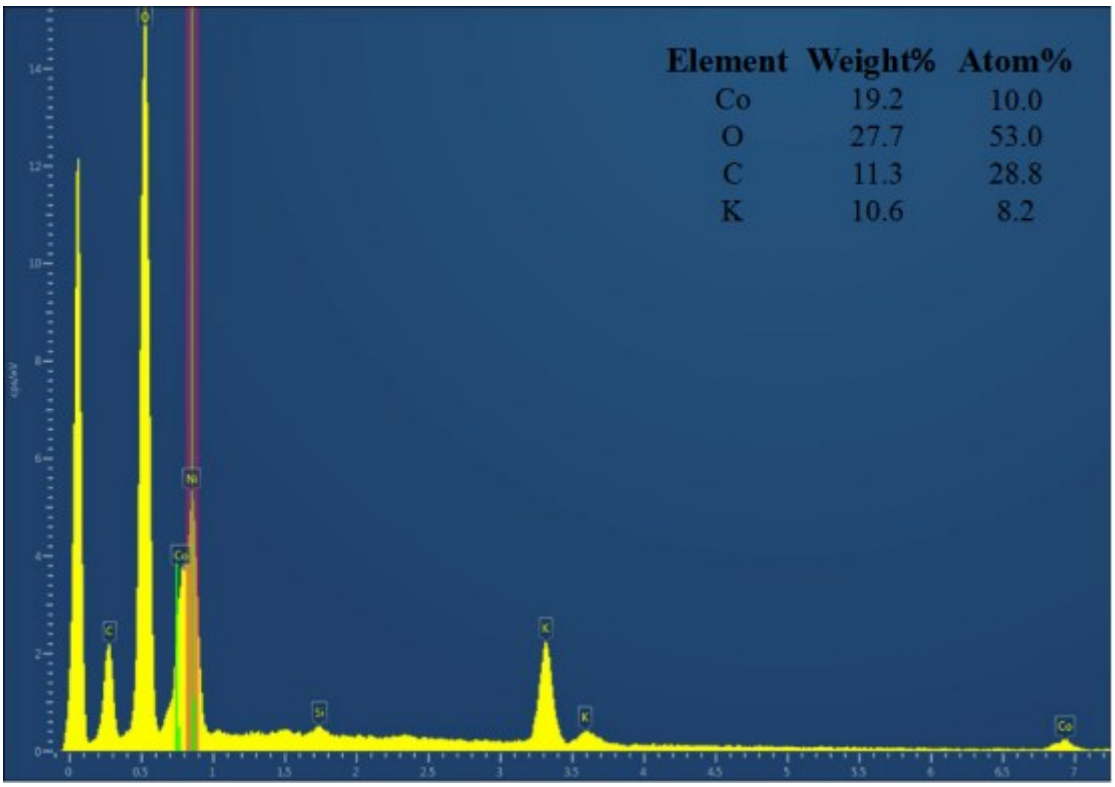

(b)

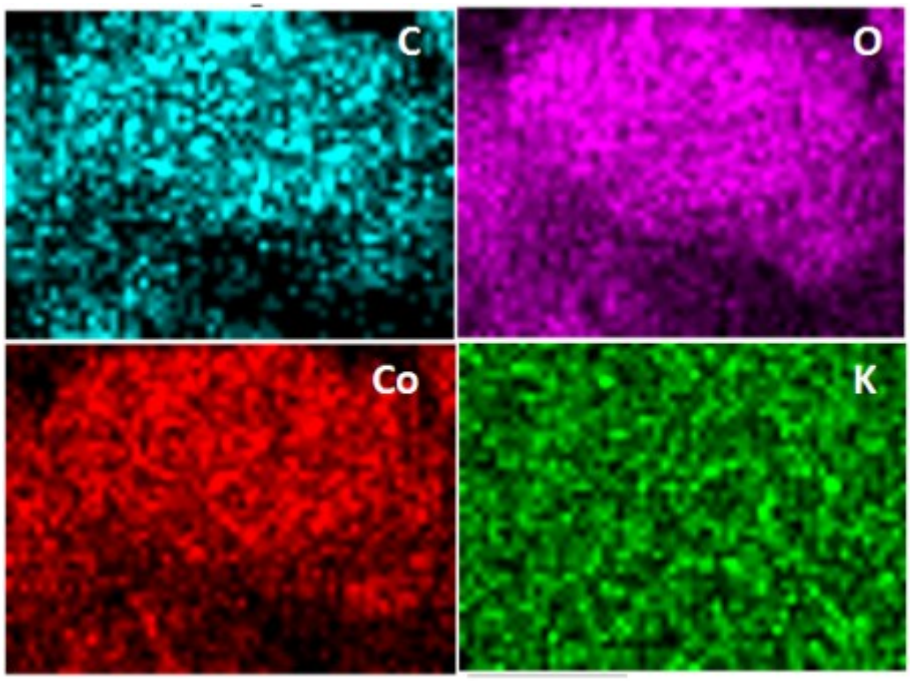

(c)

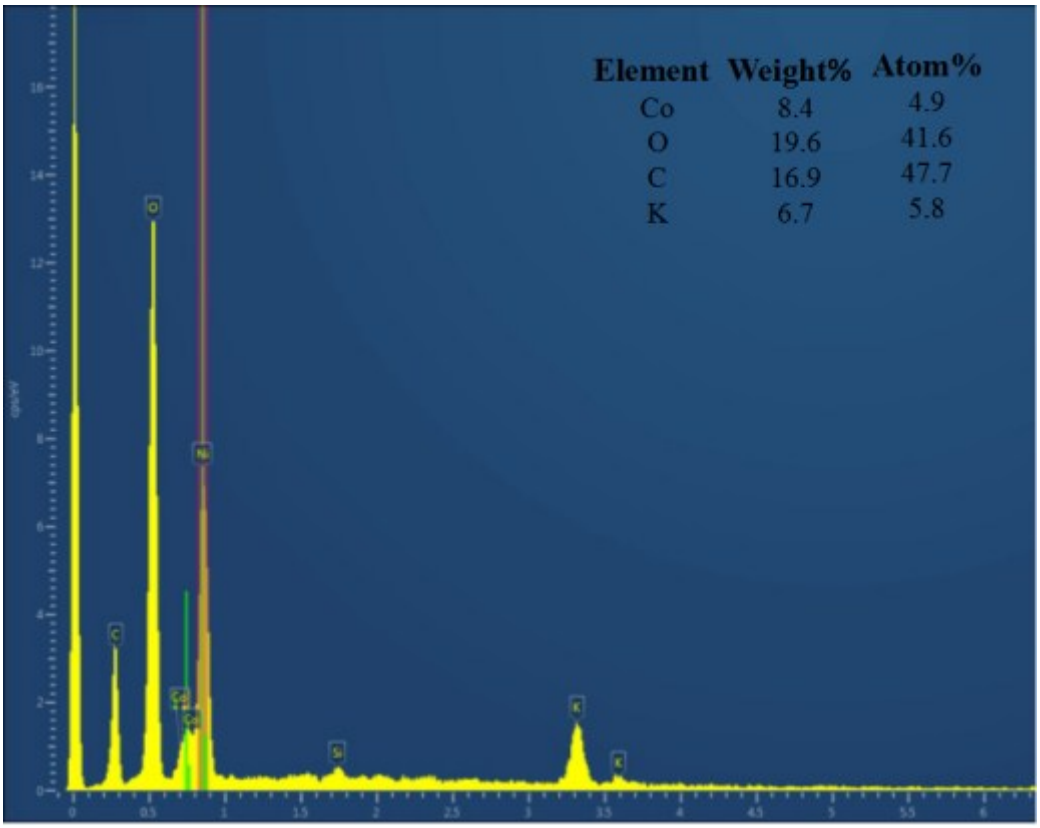

(d)

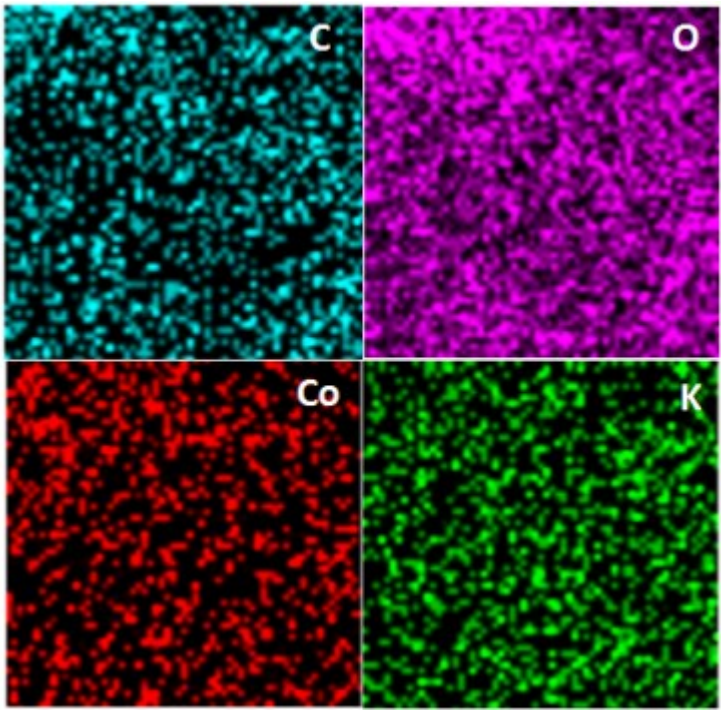

Fig. S16 EDS **(a, c)** and the Co, C and K elemental mappings for the Co_9S_8@CoS@CoO@C NPs after the 12h-electrolysis experiment **(b, d).**

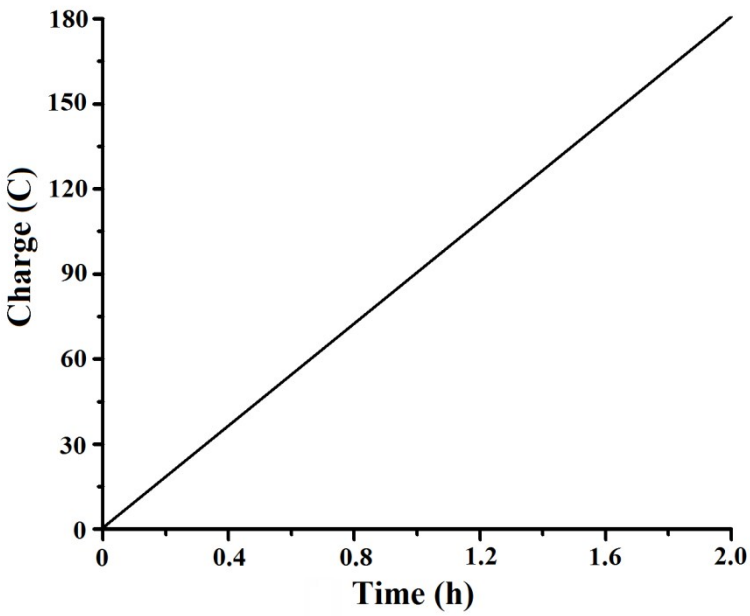

Fig. S17 Controlled potential electrolysis of the sample-modified Ni foam (sample loading: 3.6 mg·cm^{-2}) in 1M KOH aqueous solution, showing charge buildup versus time with an applied potential of 1.72 V vs. RHE (overpotential η = 0.49 V) for 2 hours.

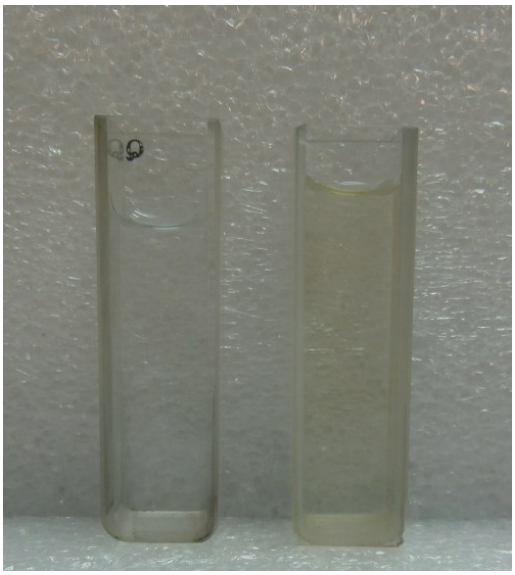

Fig. S18 Optical images of the electrolyte solution before (**left**) and after (**right**) the electrolysis experiment.

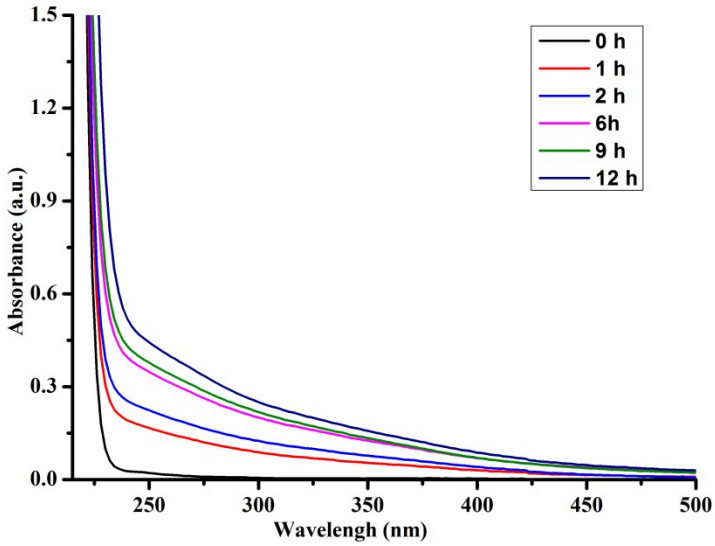

Fig. S19 UV-visible absorption spectra of the electrolyte solution before and after the electrolysis experiments with different times.

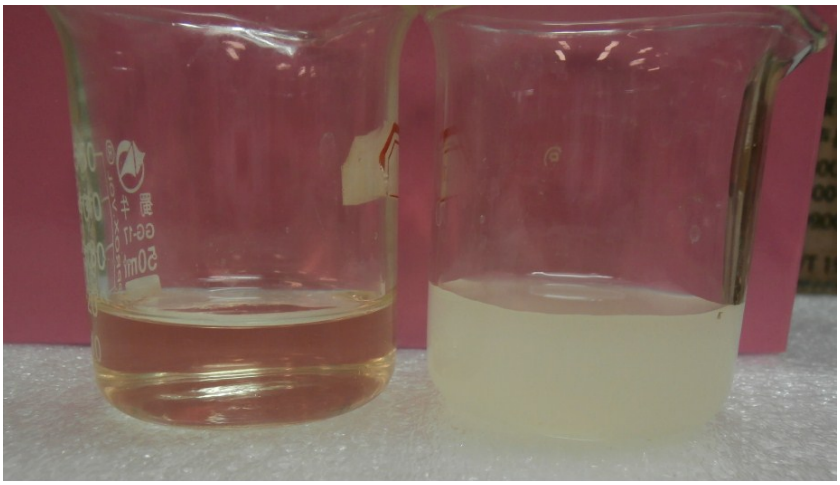

Fig. S20 Optical images of the electrolyte solution before (**left**) and after (**right**) the addition of $Ba(NO_3)_2$ saturated aqueous solution.

(a)

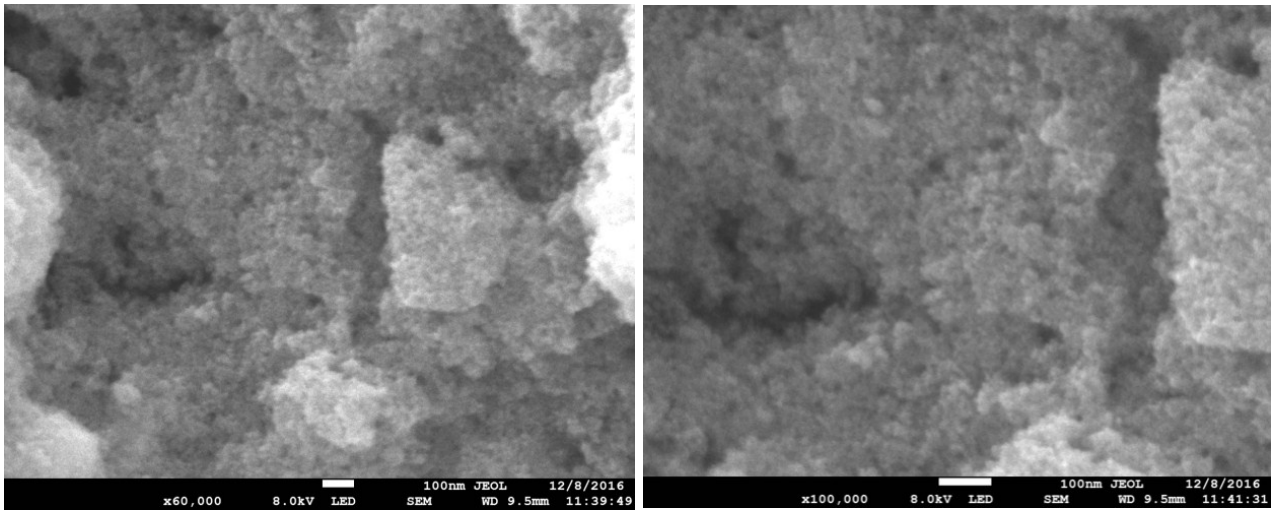

(b)

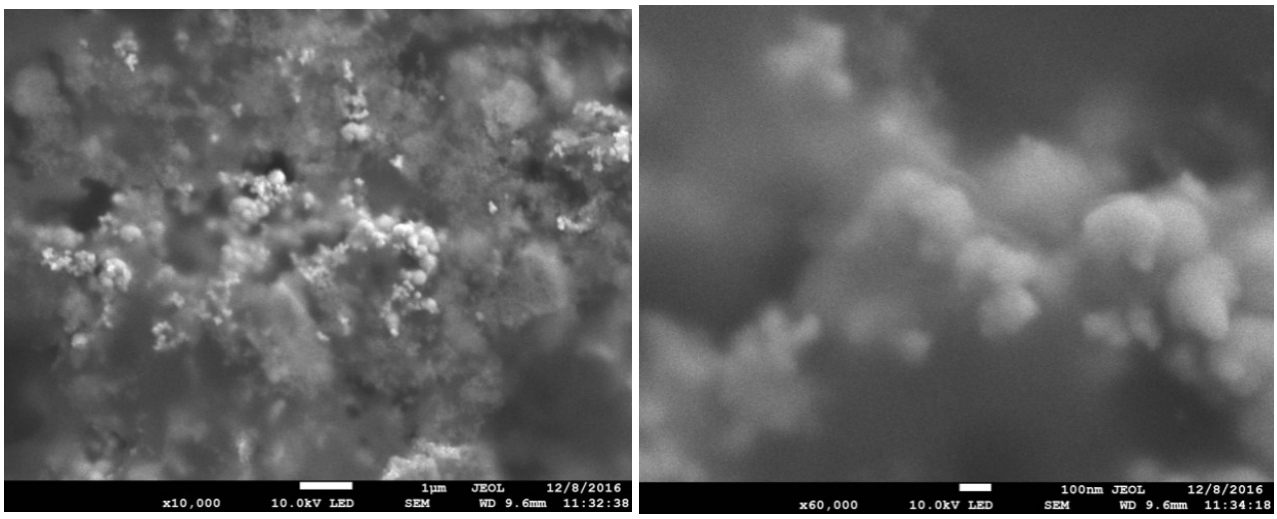

(c)

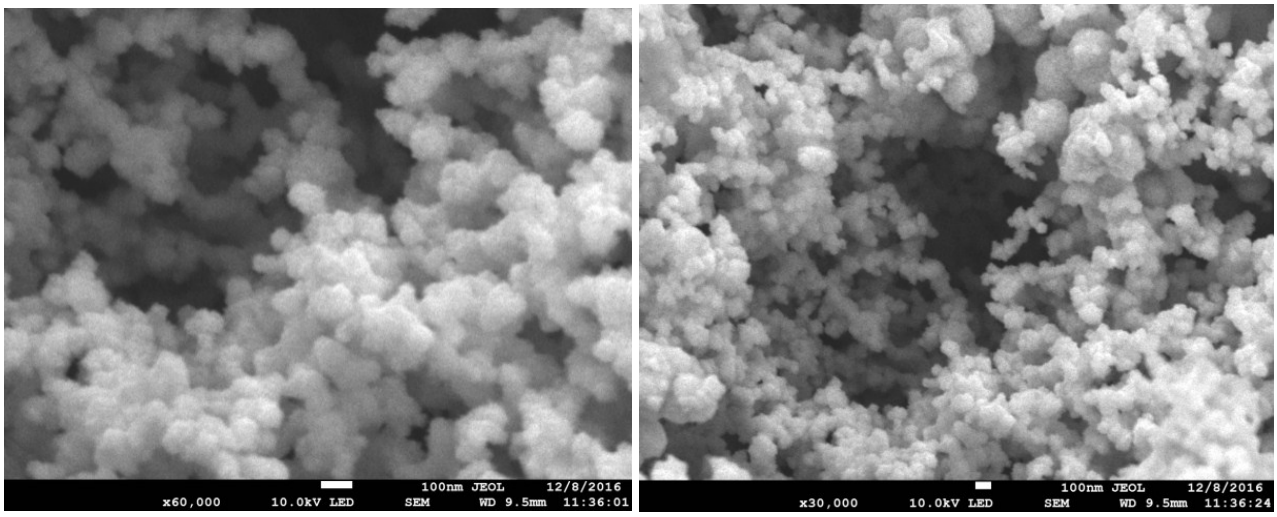

(d)

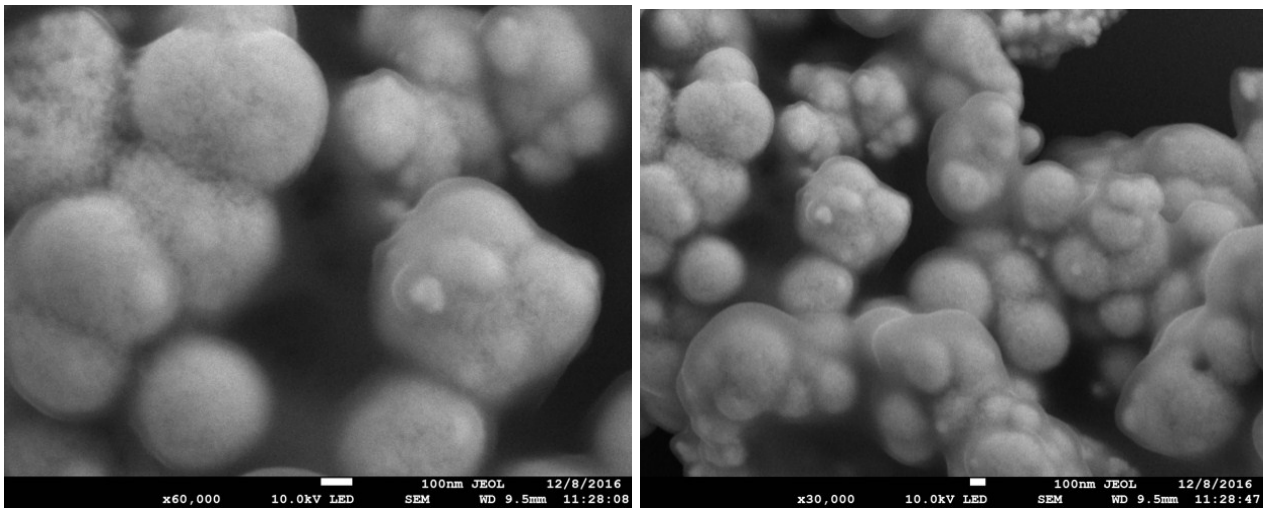

Fig. S21 The SEM images of the RuO_2 (**a**, **b**) and Pt (**c**, **d**) before (**a**, **c**) and after (**b**, **d**) the 6h-electrolysis experiment.

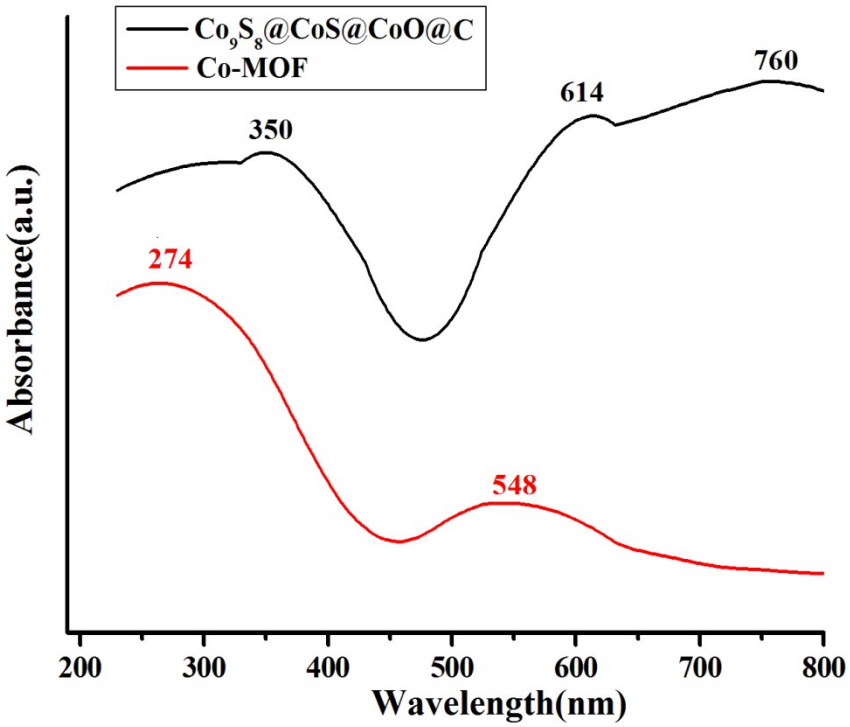

Fig. S22 UV-vis absorption spectra for the Co-MOF and Co_9S_8@CoS@CoO@C NPs in the solid state.

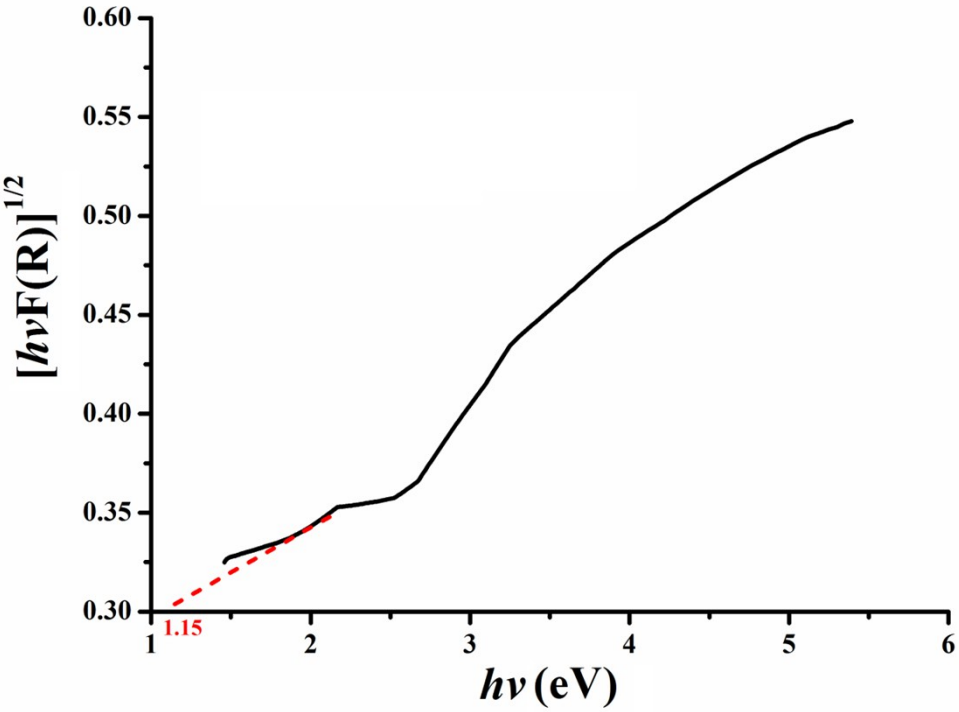

Fig. S23 The diffuse reflectance spectrum of the Co_9S_8@CoS@CoO@C NPs in transformed Kubelka–Munk function.

The diffuse reflectance spectrum of the Co_9S_8@CoS@CoO@C sample is shown in **Figure S13**. The correlation between the absorption coefficient of allowed indirect semiconductor and optical band gap E_{gap} can be determined by the equation

$$\alpha E \approx A_1(E-E_{gap})^2 \qquad (1)$$

where $E = h\nu$ is the photon energy, A_1 is a constant.

F(R) is the Kubelka−Munk equation, which is expressed as

$$F(R) = (1-R)^2/2R = k/s \qquad (2)$$

where R is the experimentally observed reflectance of the sample, k is the molar absorption coefficient, and s is the scattering coefficient. The scattering coefficients are weakly dependent on the wavelength of the incident light, and using eqs 1 and 2, the following eq 3 can be obtained:

$$[h\nu F(R)]^{1/2} = A_2[h\nu - E_{gap}] \qquad (3)$$

From the plot of $[h\nu F(R)]^{1/2}$ versus $h\nu$, by extrapolating the linear fitted regions to $[h\nu F(R)]^{1/2}=0$, the value of optical band gap of the Co_9S_8@CoS@CoO@C sample is ca. 1.15 eV.

(a)

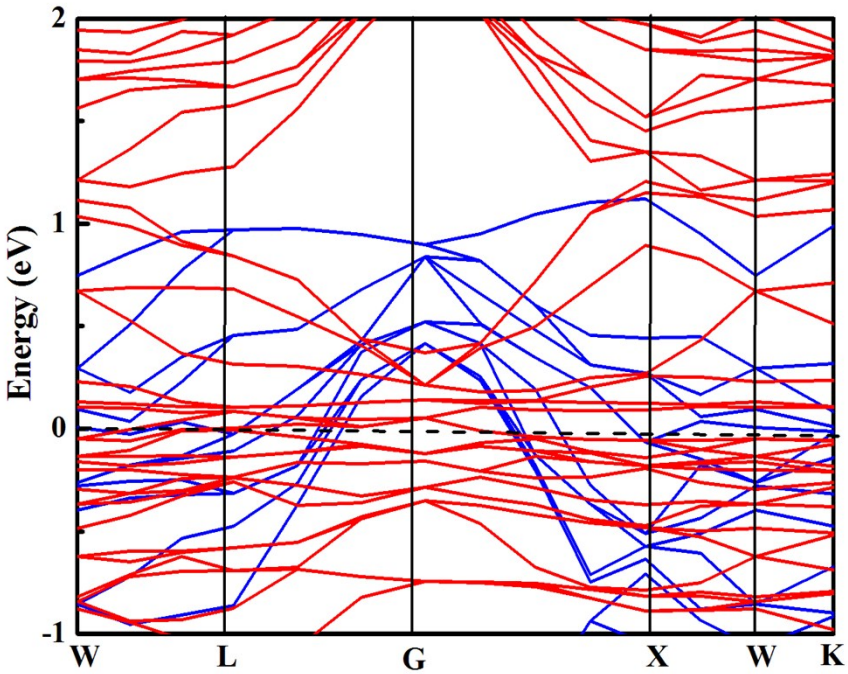

(b)

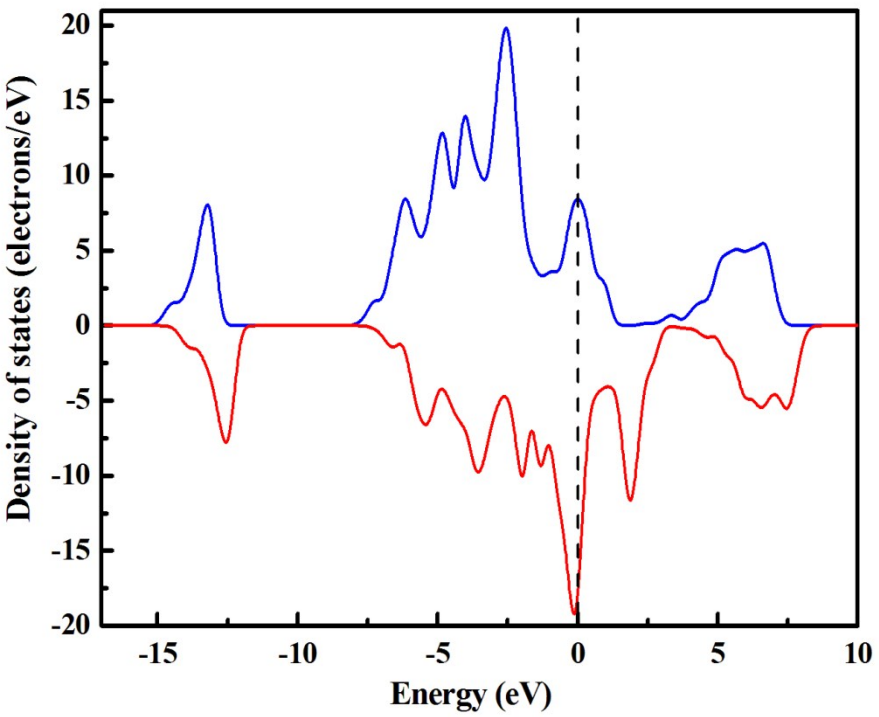

Fig. S24 The electronic band structure of the spin-polarized Co_9S_8, the blue and red curves correspond to the spin up and down bands, respectively (**a**); The corresponding DOS of the Co_9S_8 for the majority spin (blue) and the minority spin (red) (**b**). The Fermi level is set to zero.

(a)

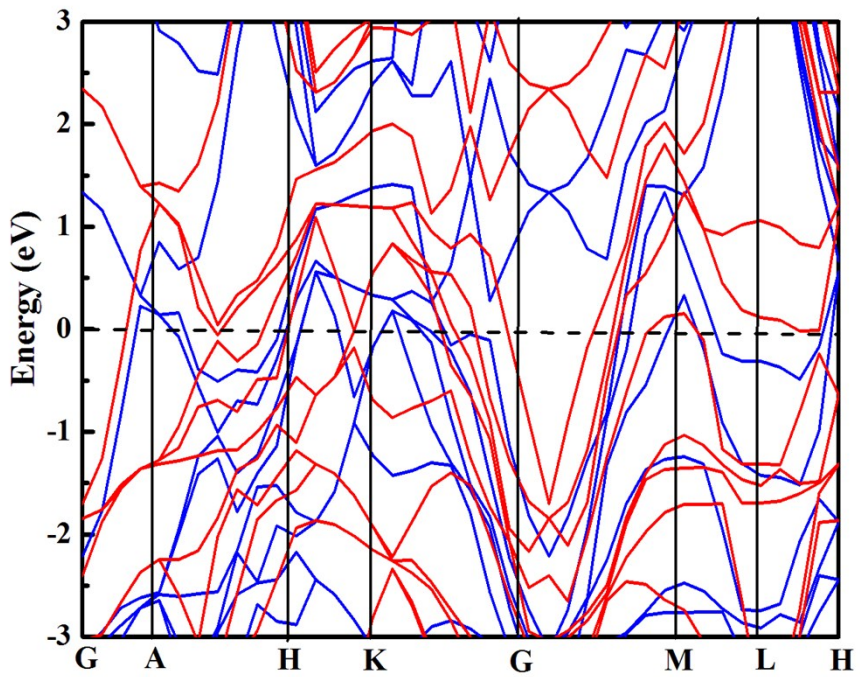

(b)

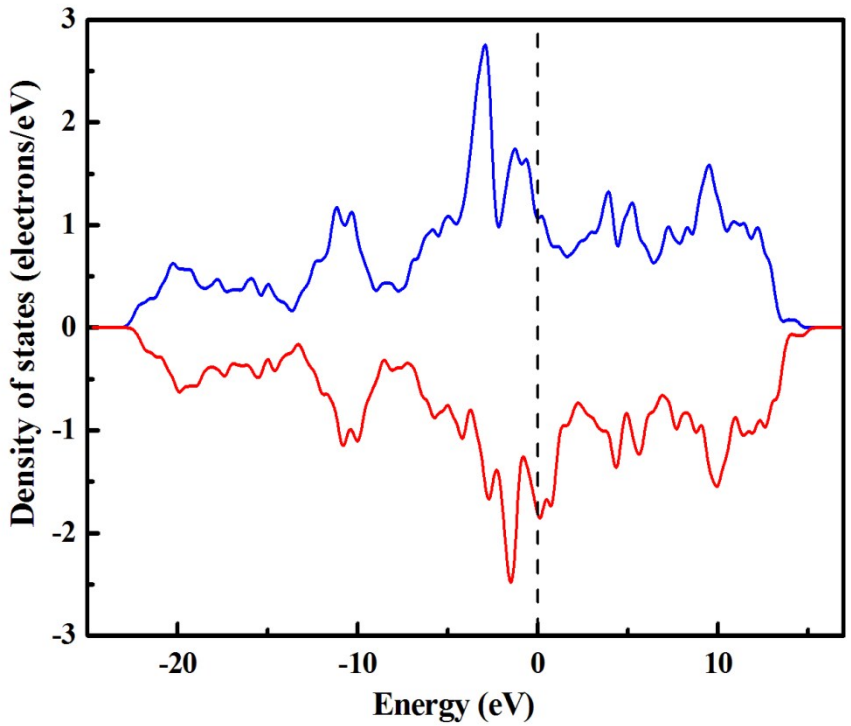

Fig. S25 The electronic band structure of the spin-polarized CoS, the blue and red curves correspond to the spin up and down bands, respectively (**a**); The corresponding DOS of the CoS for the majority spin (blue) and the minority spin (red) (**b**). The Fermi level is set to zero.

(a)

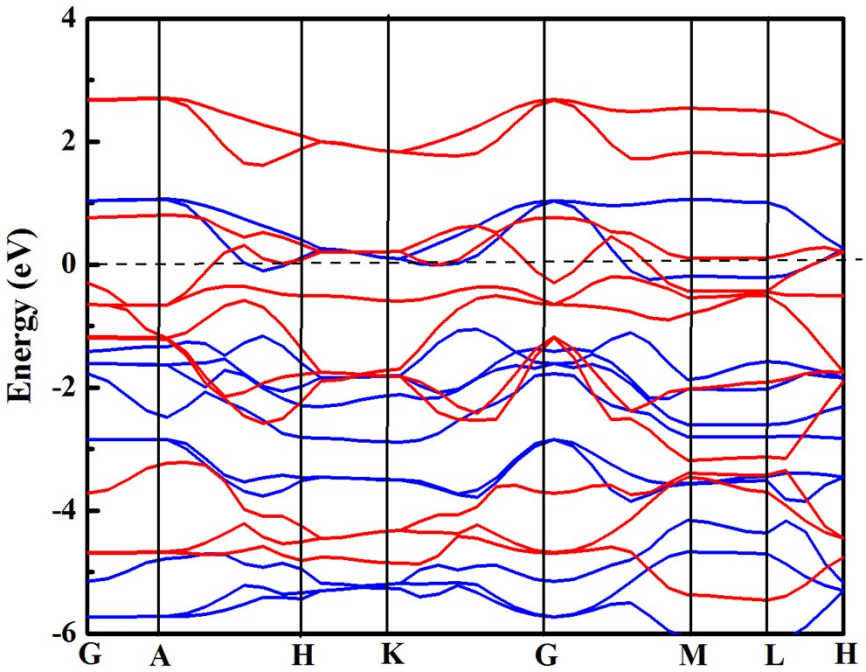

(b)

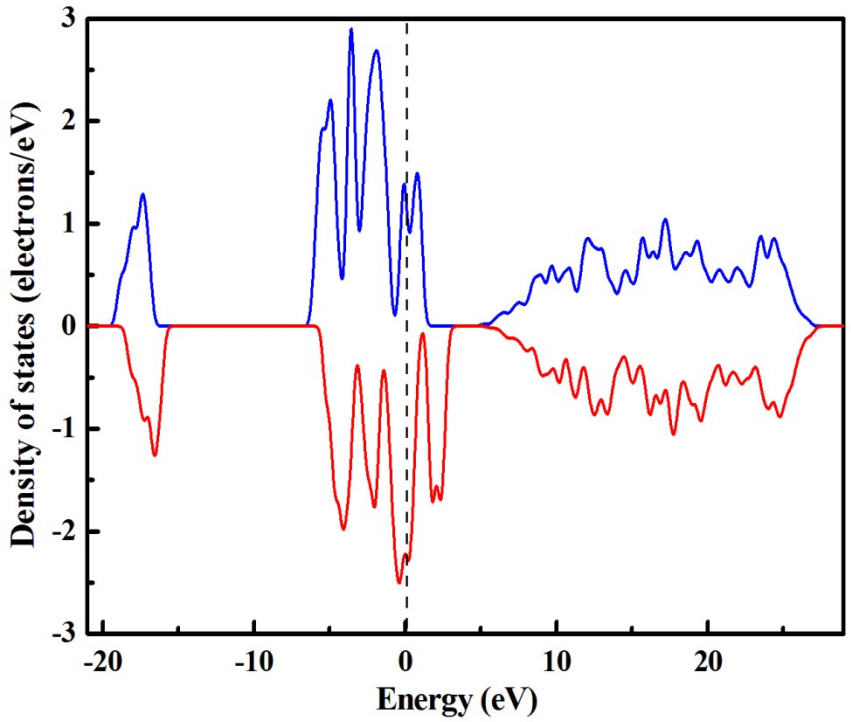

Fig. S26 The electronic band structure of the spin-polarized $Co(OH)_2$, the blue and red curves correspond to the spin up and down bands, respectively (**a**); The corresponding DOS of the CoS for the majority spin (blue) and the minority spin (red) (**b**). The Fermi level is set to zero.

(a)

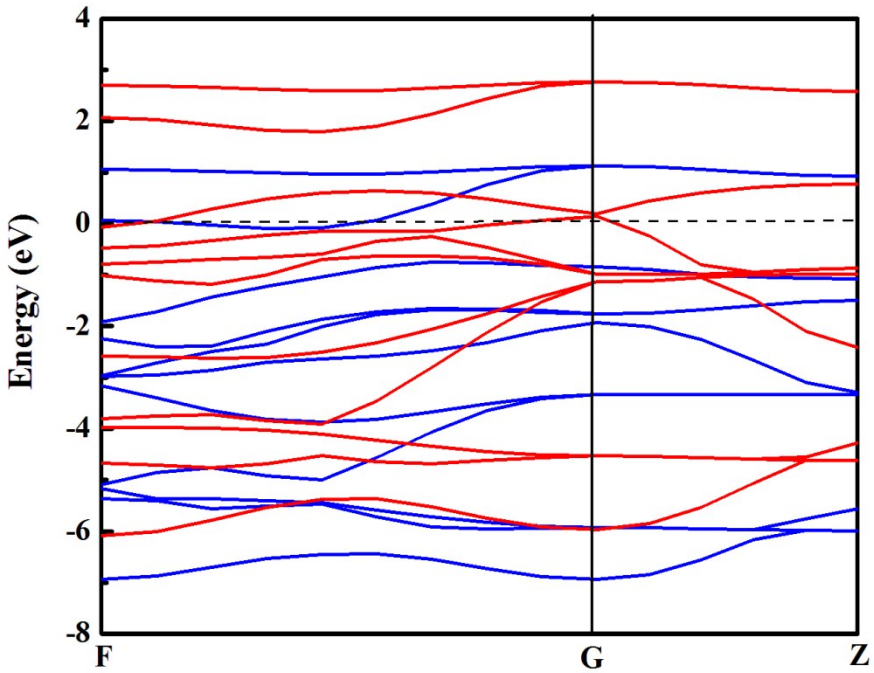

(b)

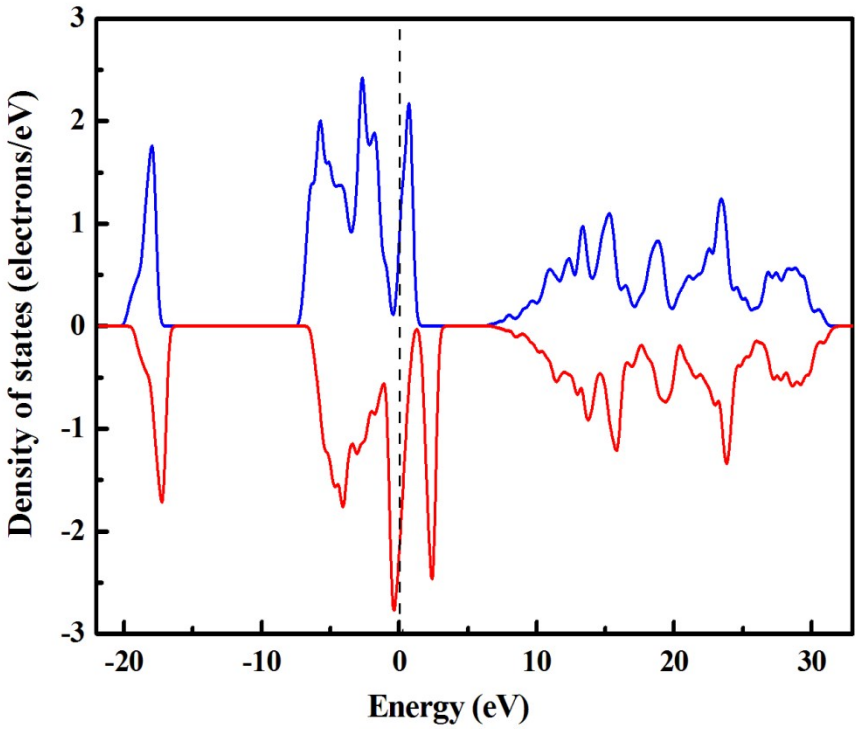

Fig. S27 The electronic band structure of the spin-polarized CoOOH, the blue and red curves correspond to the spin up and down bands, respectively (**a**); The corresponding DOS of the CoOOH for the majority spin (blue) and the minority spin (red) (**b**). The Fermi level is set to zero.

(a)

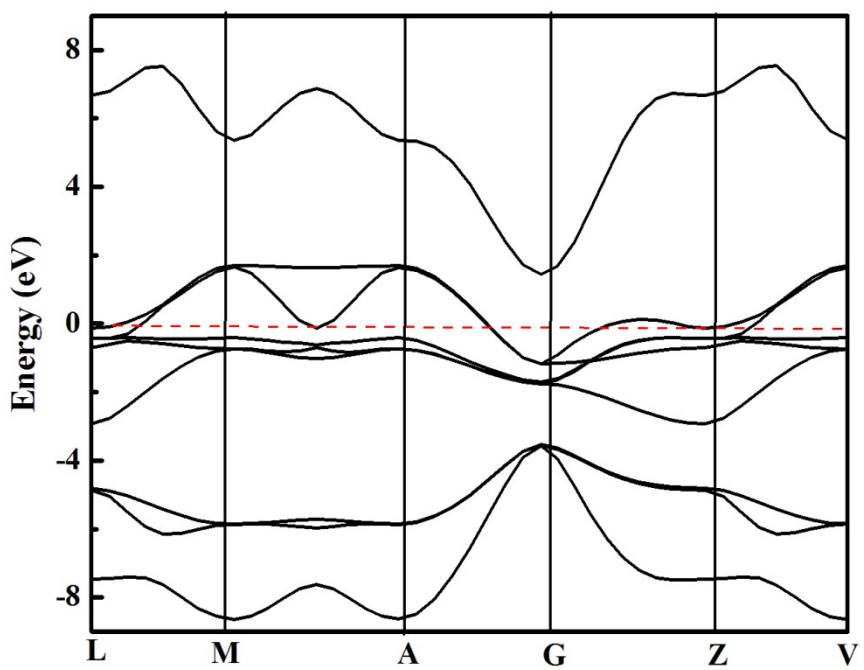

(b)

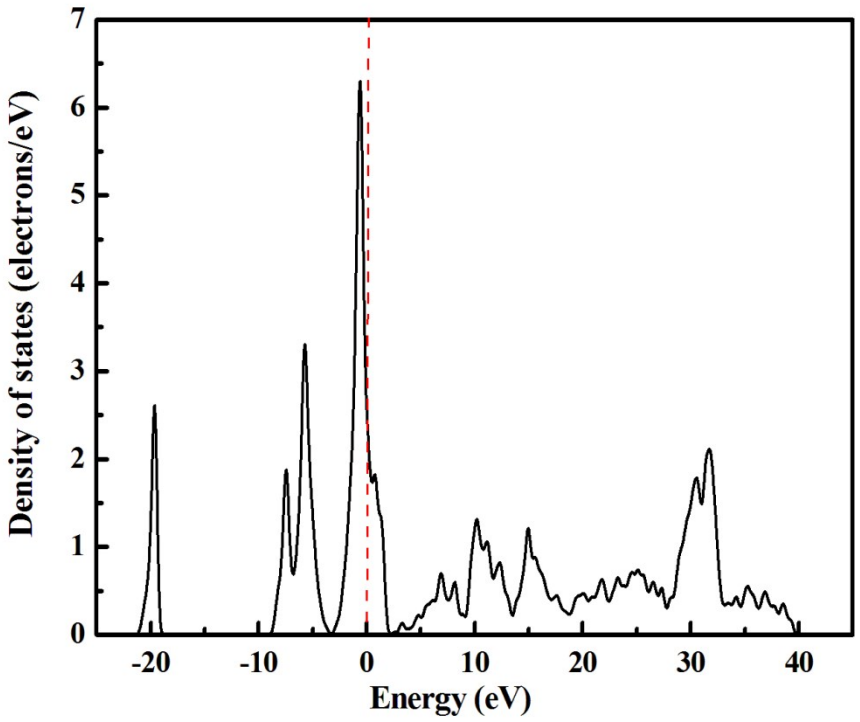

Fig. S28 The electronic band structure (**a**) and TDOS (**b**) of the spin-unpolarized CoO.

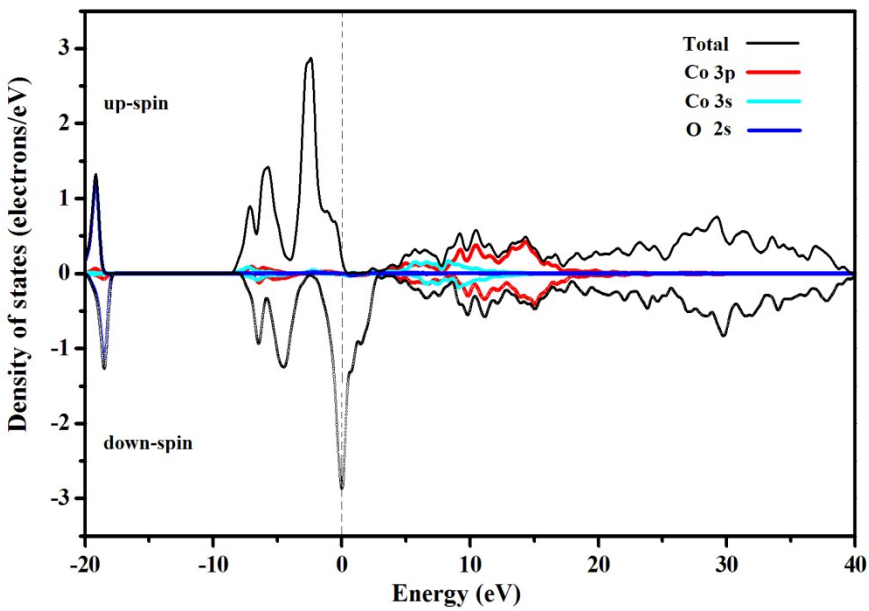

Fig. S29 The calculated TDOS (black) and PDOS of the spin-polarized CoO. The positive and negative values express the spin-up and spin-down states, respectively. In the PDOS, red, sapphire and blue lines represent Co 3p, Co 3s and O 2s states, respectively (**b**). The Fermi level is set to zero.

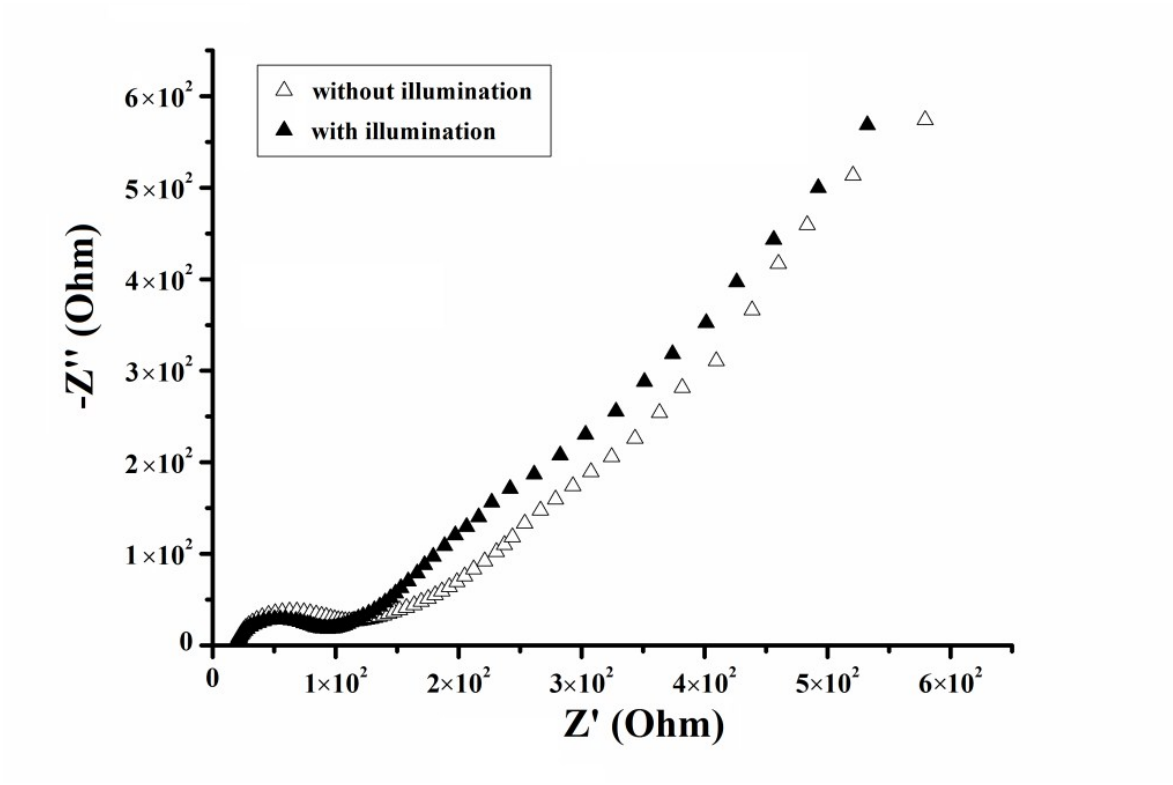

Fig. S30 Nyquist plots of the Co_9S_8@CoS@CoO@C NPs at E = 1.07 V vs RHE with and without the visible light irradiation (650 nm > λ > 350 nm, 100 mW·cm^{-2}).

References

1 M. R. Gao, W. C. Sheng, Z. B. Zhuang, Q. R. Fang, S. Gu, J. Jiang and Y. S. Yan, *J. Am. Chem. Soc.*, 2014, **136**, 7077.